Non-canonical mTOR-Independent Role of DEPDC5 in Regulating GABAergic Network Development

Amrutha Swaminathan, Rahma Hassan-Abdi, Solène Renault, Aleksandra Siekierska, Raphaëlle Riché, Meijiang Liao, Peter de Witte, Constantin Yanicostas, Nadia Soussi-Yanicostas, Pierre Drapeau, et al.

Current Biology

Non-canonical mTOR-independent role of DEPDC5 in regulating GABAergic network development

--Manuscript Draft--

Manuscript Number:	CURRENT-BIOLOGY-D-17-01554R3
Full Title:	Non-canonical mTOR-independent role of DEPDC5 in regulating GABAergic network development
Article Type:	Research Article
Corresponding Author:	Eric Samarut, Ph.D CRCHUM Montreal, CANADA
First Author:	Amrutha Swaminathan
Order of Authors:	Amrutha Swaminathan
	Rahma Hassan-Abdi
	Solene Renault
	Aleksandra Siekierska
	Raphaelle Riche
	Meijiang Liao
	Peter A.M de Witte
	Constantin Yanicostas
	Nadia Soussi-Yanicostas
	Pierre Drapeau
	Eric Samarut, Ph.D
Abstract:	Mutations in DEPDC5 are causal factors for a broad spectrum of focal epilepsies, but the underlying pathogenic mechanisms are still largely unknown. To address this question, a zebrafish depdc5 knockout model showing spontaneous epileptiform events in the brain, increased drug-induced seizure susceptibility, general hypoactivity and premature death at 2-3 weeks post fertilization as well as the expected hyperactivation of mTOR signaling was developed. Using this model, the role of DEPDC5 in brain development was investigated using an unbiased whole transcriptomic approach. Surprisingly, in addition to mTOR-associated genes, many genes involved in synaptic function, neurogenesis, axonogenesis and GABA network activity were found to be dysregulated in larval brains. Although no gross defects in brain morphology/neuron loss were observed, immunostaining of depdc5-/- brains for several GABAergic markers revealed specific defects in the fine branching of GABAergic network. Consistently, some defects in depdc5-/- could be compensated by treatment with GABA, corroborating that GABA signaling is indeed involved in DEPDC5 pathogenicity. Further, the mTOR-independent nature of the neurodevelopmental defects was demonstrated by the inability of rapamycin to rescue the defects of GABAergic networks observed in depdc5-/- brains and conversely, the inability of GABA to rescue the hypoactivity in another genetic model showing mTOR hyperactivation. This study hence provides the first in vivo evidence that DEPDC5 plays previously unknown roles apart from its canonical function as an mTOR inhibitor. Moreover, these results propose that defective neurodevelopment of GABAergic network could be a key factor in epileptogenesis when DEPDC5 is mutated.

Graphical Abstract

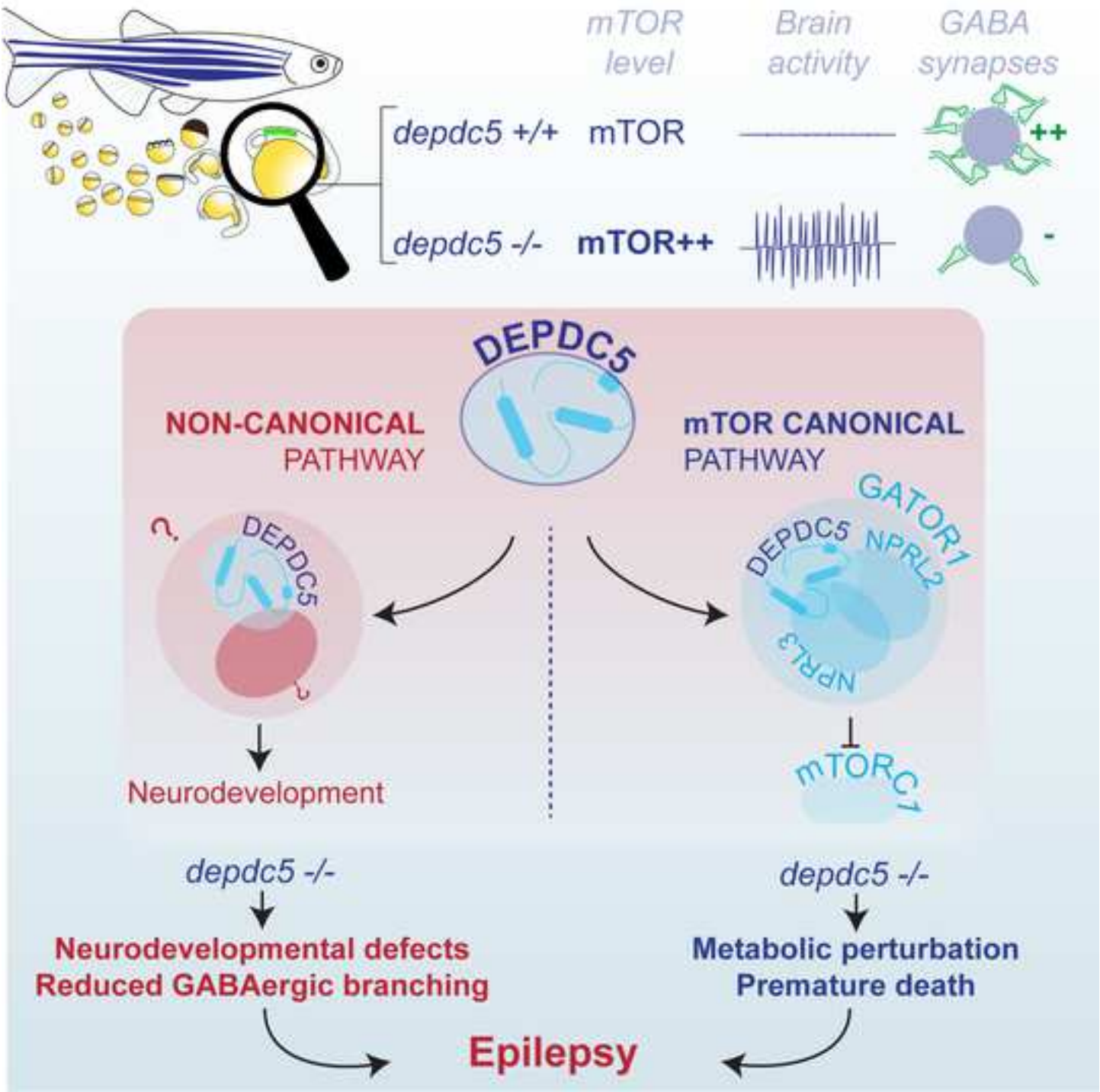

Non-canonical mTOR-independent role of DEPDC5 in regulating GABAergic network development.

Amrutha Swaminathan[1], Rahma Hassan-Abdi[2,3], Solène Renault[2,3], Aleksandra Siekierska[4], Raphaëlle Riché[1], Meijiang Liao[1], Peter A.M. de Witte[4], Constantin Yanicostas[2,3], Nadia Soussi-Yanicostas[2,3], Pierre Drapeau[1,5#] and Éric Samarut[1,5,#]

[1] Department of Neurosciences, Research Center of the University of Montréal Hospital Center (CRCHUM), Université de Montréal, Montréal, Canada H2X0A9.

[2] Inserm, U1141, F-75019 Paris, France

[3] Université Paris Diderot, Sorbonne Paris Cité, UMRS 1141, F-75019 Paris, France

[4] Laboratory for Molecular Biodiscovery, Department of Pharmaceutical and Pharmacological Sciences, University of Leuven, 3000 Leuven, Belgium

[5] DanioDesign Inc., Montréal, Canada.

[#] Co-corresponding authors: p.drapeau@umontreal.ca and eric.samarut@umontreal.ca

Lead contact: Éric Samarut (eric.samarut@umontreal.ca)

Running title: DEPDC5 regulates GABA network development

Summary

Mutations in *DEPDC5* are causal factors for a broad spectrum of focal epilepsies, but the underlying pathogenic mechanisms are still largely unknown. To address this question, a zebrafish *depdc5* knockout model showing spontaneous epileptiform events in the brain, increased drug-induced seizure susceptibility, general hypoactivity, premature death at 2-3 weeks post fertilization as well as the expected hyperactivation of mTOR signaling was developed. Using this model, the role of DEPDC5 in brain development was investigated using an unbiased whole transcriptomic approach. Surprisingly, in addition to mTOR-associated genes, many genes involved in synaptic function, neurogenesis, axonogenesis and GABA network activity were found to be dysregulated in larval brains. Although no gross defects in brain morphology/neuron loss were observed, immunostaining of *depdc5*-/- brains for several GABAergic markers revealed specific defects in the fine branching of GABAergic network. Consistently, some defects in *depdc5*-/- could be compensated for by treatment with GABA, corroborating that GABA signaling is indeed involved in DEPDC5 pathogenicity. Further, the mTOR-independent nature of these neurodevelopmental defects was demonstrated by the inability of rapamycin to rescue the GABAergic network defects observed in *depdc5*-/- brains and conversely, the inability of GABA to rescue the hypoactivity in another genetic model showing mTOR hyperactivation. This study hence provides the first *in vivo* evidence that DEPDC5 plays previously unknown roles apart from its canonical function as an mTOR inhibitor. Moreover, these results propose that defective neurodevelopment of GABAergic networks could be a key factor in epileptogenesis when *DEPDC5* is mutated.

Keywords: Epilepsy/DEPDC5/GABA/mTOR/Neurodevelopment/zebrafish

Introduction:

Focal seizures, which originate in one part of the brain, are the most prevalent type of epileptic seizures and mutations in *DEPDC5* (Dishevelled, Egl-10 and Pleckstrin (DEP)-domain containing 5) account for 12-37% of the cases [1]. Though numerous ion channel mutations have been traditionally associated with epilepsy, recent work using whole genome/exome sequencing has identified other pathways in epilepsy, like mTOR (mechanistic/mammalian target of rapamycin) signaling. The causative gene for familial focal epilepsy with variable foci (FFEVF) remained unknown until the identification of *DEPDC5* mutations in a large number of families with FFEVF [2-4]. Mutations in *DEPDC5* leading to haploinsufficiency have been associated also to other focal epilepsies including autosomal dominant nocturnal frontal lobe epilepsy and familial temporal lobe epilepsy [3, 5].

DEPDC5, along with NRPL2 and NRPL3 forms the mTOR inhibitory GATOR1 complex, which blocks the activation of the classical mTOR complex, mTORC1, when amino acid concentration is low [6]. Mutations in all three components have been linked to focal epilepsy with/without cortical malformations [7-10]. The mTOR pathway plays a significant role in the regulation of protein synthesis and in critical cell fate decisions like autophagy. Absence of regulation of this pathway results in constitutively high mTORC1 activity, and mTOR hyperactivation has been implicated in various neurological conditions associated with intractable seizures [11]. Thus, mTOR inhibitors like rapamycin and its analogs hold significant potential in anti-epileptogenic therapies [12, 13].

Since the components of the GATOR1 complex have only been recently associated with epilepsy, their pathophysiological roles related to focal epilepsy are yet to be completely understood. Moreover, some initial discoveries found that multiple *DEPDC5* mutations in

patients are located in a domain of unknown function (DUF3608) [3], thus suggesting that unexpected roles of DEPDC5 may be associated with its pathogenicity. There are three rodent models of DEPDC5 knockout, where homozygotes show mTOR hyperactivation, severe morphological defects and premature death [14-16]. The conditional knockout mouse model reported recently describes cortical defects and increased seizure susceptibility in adult mice recapitulating many features of mTORopathies [16]. However, in order to investigate the function of DEPDC5 during neurodevelopment, new animal models more conducive to the study of early development are required, and hence, we used zebrafish as a handy neurodevelopmental model.

In this study, we report the generation and use of a zebrafish model of DEPDC5 loss-of-function to understand the underlying pathological mechanisms. This *depdc5* knockout model showed mTOR hyperactivation, behavioral hypoactivity, spontaneous epileptiform brain events, increased drug-induced seizure susceptibility and premature death. An unbiased transcriptomic analysis of the brains of *depdc5-/-* larvae was performed which showed that, apart from the metabolic perturbation occurring due to mTOR hyperactivation, the regulation of neurodevelopmental pathways was also affected. In particular, fine branching of the GABA network was specifically affected by DEPDC5 knockout. Consistently, treatment with GABA could compensate for some of the defects. Further, these neurodevelopmental changes as well as the transcriptomic changes induced by DEPDC5 knockout occur independently of mTOR signaling. As a result, this study presents new evidence that DEPDC5 is not only involved in mTOR-dependent pathways but is also involved in previously unknown mTOR–independent functions especially during neurodevelopment, a combination of which result in focal epilepsies.

These novel insights into the function of DEPDC5 in brain development bring the first evidence of how DEPDC5 loss-of-function could lead to epilepsy.

Results:

Depdc5 is essential for vertebrate survival

Though *DEPDC5* mutations were associated with epilepsy, the underlying pathology of this class of focal epilepsies remains unstudied. Zebrafish has only one ortholog of DEPDC5, and sequence alignment of the zebrafish and human proteins showed a high degree of conservation with 75% identity and 84% similarity. Whole mount RNA *in situ* hybridization showed that *depdc5* is expressed in the forebrain, midbrain, hindbrain and also in the neural tube and notochord during zebrafish development (Figure 1A).

Using CRISPR/Cas9 genome editing, the 14th exon of *depdc5* encoding the DUF3608, which was initially found to be mutated in many patients [2, 17], was targeted for disruption. A positive founder transmitting a 4-nucleotide frame-shifting deletion was selected, which would lead to the expression a truncated protein (352 amino acids instead of the 1568 residue wild-type protein, Figure 1B). Quantification of mRNA expression showed significant reduction in heterozygous and homozygous larvae (Figure 1C). Since crosses of heterozygotes never resulted in viable juvenile/adult homozygotes, according to the 1:2:1 Mendelian ratio, the survival of all the three genotypes: *depdc5*+/+ (wild type), *depdc5*+/- and *depdc5*-/- was monitored for a month from 0 day post fertilization (dpf). While most of the *depdc5*+/+ and +/- larvae survived for this period, all the *depdc5*-/- larvae died by two weeks of age (Figure 1D). Notably, the survival of *depdc5*-/- can be extended by few days if they are separated early and raised with extra care, although they never survive after 20 dpf. However, no obvious morphological defects

or changes in eye size were observed, though a small reduction in body length was seen following quantification (Figures 1E and 1F). While this observation is consistent with the premature death of rodent *Depdc5-/-* models [14-16], the growth delay observed in the complete knockout rodent embryos was not evident in case of *depdc5-/-* zebrafish larvae. Hence, though vertebrates can survive haploinsufficiency of DEPDC5, total absence leads to death during development.

depdc5-/- larvae show mTOR hyperactivation, brain epileptic discharges, hypoactivity and increased seizure susceptibility

Since DEPDC5 is known to negatively regulate mTOR, mTORC1 activity was assessed through the phosphorylation state of the ribosomal protein S6, which is a downstream effector of mTORC1 [18]. Lysates of 8 dpf *depdc5+/+*, *depdc5+/-* and *depdc5-/-* larvae were analyzed by western blotting using antibodies against the S6 Ser240/244 phospho-epitope, and a gradual increase in the phosphorylation was observed (Figure 2A), indicating high mTORC1 activity in the absence of DEPDC5. This was confirmed by performing immunohistological analysis where *depdc5-/-* larval brains showed greater levels of phospho-S6 (Figure 2B). However, no abnormal or dysmorphic cells were visible. In order to monitor epileptic activity, brain activity was monitored using non-invasive local field potential (LFP) recordings from the optic tectum [19]. Recurrent spontaneous epileptiform events were observed in *depdc5-/-* larval brains at 9 dpf (Figures 2C and 2D) at a mean frequency of 9.1 $\pm$ 5.0 events/10 minutes and mean duration of 309.7 $\pm$ 152.3 msec, confirming the pathogenicity of DEPDC5 loss-of-function. However, since the LFPs were monitored only for 10 minutes, this epileptic brain activity was observed in only 9/42 larvae, and it is possible that many larvae show epileptiform discharges outside this period. Nevertheless, no such events were recorded in different batches of *depdc5+/+* (0 out of 40

larvae). It is also possible that these epileptiform discharges manifest earlier but were only monitored at 9 dpf in order to increase the chances of detecting them. The absence of epileptiform discharges in 100% of the animals is consistent with similar observations in *Depdc5* conditional knockout mice and patients with focal epilepsy [16]. In order to have a more accurate readout of the abnormalities in *depdc5-/-* larvae, their locomotor activity was quantified in light-dark cycles. *depdc5-/-* larvae were significantly hypoactive (Figure 2E), and this was observed in 100% of the larvae across generations from 5 dpf onward (N>5; n>300), till before death. These results are also consistent with other mTORopathy zebrafish models which show epileptic brain activity and are hypoactive [20]. Interestingly, when coiling (rotating movement of embryo inside the chorion) was monitored at 20 hpf, this earliest motor behavior was already lower in *depdc5-/-* embryos (Figure 2F), indicating that the hypoactivity begins very early during development, suggesting that DEPDC5 loss-of-function may have consequences on early neurodevelopment. Lastly, the susceptibility of *depdc5-/-* larvae to chemically-induced seizures by pentylenetetrazol (PTZ) was tested. Consistently with what have been reported in mice [16], *depdc5-/-* larvae show a significantly increased response to PTZ (shorter delay of response to PTZ exposure and higher swimming activity) compared to their siblings (Figure 2G and 2H).

Altogether, the phenotypes observed upon knocking out *depdc5* in zebrafish are reminiscent of what is observed in the existing rodent models of *Depdc5* knockout and also to an extent, in patients. Altogether, these results validate the pathogenicity of *depdc5* loss-of-function in zebrafish.

Alteration of brain gene expression profile in *depdc5-/-*

In order to obtain new unbiased insights into the molecular perturbations occurring during neurodevelopment in the absence of DEPDC5, brains of 10 dpf *depdc5*+/+ and -/- larvae were dissected out and total RNA was extracted for deep sequencing (Figure 3A). This age was chosen as an intermediate stage to perform exhaustive analysis of the molecular phenotype at a stage when the swimming phenotype is distinct, while preventing the perturbation of gene expression by the premature death that occurs 5 days later. From the differential gene expression analysis, 1191 genes out of approximately 12,000 genes expressed in the larval brain were found to be significantly up- (532 genes) or downregulated (659 genes) ($p<0.05$) (full list can be found in Table S1, description provided for top dysregulated genes). Notably, 16 out of the 20 aminoacyl-tRNA synthetases in zebrafish were upregulated in the *depdc5*-/- brains, presumably due to improper mTOR regulation. Functional annotation and clustering of the significantly dysregulated genes showed that apart from aminoacyl-tRNA biosynthesis and electron transport chain that can be attributed to mTOR pathway dysfunction, the expression of genes involved in other pathways including chordate embryonic pattern specification, regulation of neuron projection morphogenesis/axonogenesis, synapse formation, zinc finger/transcription factors and ion channels were also perturbed (Figure 3B). This suggested that DEPDC5 may also play a role in embryonic neurodevelopment.

Since genes related to neurodevelopment were altered, the number of neurons during developmental stages was analyzed. Measurement of the head size and staining with cresyl violet showed that the size and morphology of *depdc5*-/- larval brains were similar to that of the control (Figures 3D and 3F). In addition, using immunostaining against acetylated tubulin and phosphorylated histone H3 (which label neuronal fibres and mitotic cells respectively), the main brain networks and neurogenesis itself did not appear to be affected (Figures 3C and 3E).

However, many genes related to GABAergic networks which have conventionally been correlated with other kinds of epilepsy, were downregulated. Indeed, 3 GABA receptors (GABRA1, GABBR1b and GABRG2) and other associated factors required for synthesis and transport of GABA, GABAergic synapse formation, maturation and transmission (like Gat3, pyruvate carboxylase, Kcc2 and neuroligin 2) were all downregulated (Table S3).

Since the expression of multiple factors important for GABAergic network formation and synaptic function was perturbed, the expression of three markers of inhibitory synapses, Gad65/67, gephyrin and neurogilin-2 (Nlgn-2), was examined by immunostaining of transverse sections from 8 dpf *depdc5*+/+ and *depdc5*-/- larval brains. Interestingly, close examination of the sections immunostained with Gad65/67 showed that finer branched structures were not present as in wild type siblings (Figure 4A). 3D reconstruction of Gad65/67 staining confirmed that the Gad65/67 projections (in blue in Figure 4B) are less arborized in the mutant brains. Since GABA synthetizing enzymes are expressed in clusters at the pre-synaptic GABA synapses, these results confirm defects in the GABAergic network connectivity. Immunolabeling against gephyrin and Nlgn2 also showed a significant decrease of the complexity in *depdc5*-/- brains (Figures 4C and 4D). Upon quantifying the GAD65/67 and gephyrin positive neurofilaments and puncta from at least three biological replicates, both were decreased by >50% in *depdc5*-/- (Figure 4F). Lastly, immunolabelling and quantification of the interneuron population using parvalbumin 7 antibody did not show any difference in the number of positive cells (Figure 4E and 4F). These results demonstrate that DEPDC5 loss-of-function significantly impacts fine branching of GABAergic network during neurodevelopment without causing major loss of interneurons.

GABA exposure rescues hypoactivity and seizure susceptibility in *depdc5-/-* larvae through paracrine effects

Since the expression of GABA synthetizing enzymes seemed to be affected, we hypothesized that exposure to GABA may compensate for this decrease and could therefore rescue the consistent hypoactivity and seizure susceptibility phenotypes of *depdc5-/-* larvae. Concurrently with this hypothesis, GABA treatment could completely rescue the hypoactivity of *depdc5-/-* larvae (swimming at 7 dpf and coiling at 24 hpf) (Figures 5A and 5B). Rapamycin, which has a positive effect on other mTORopathy models, was used as a positive control, and could also completely rescue the hypoactivity of *depdc5-/-* embryos and the increased phospho-S6 levels (Figures 5A-C). Moreover, GABA treatment, as well as rapamycin could rescue the seizure susceptibility of *depdc5-/-* larvae exposed to PTZ, to the level of their siblings (Figures 5D and 5E). Hence, these results confirm earlier observations from transcriptomic and immunolabelling experiments that GABA network/signalling is indeed altered in *depdc5-/-* larvae. Moreover, it shows that both GABA and mTOR signalling are involved in the pathogenicity of *depdc5* loss-of-function.

In order to assess if this rescuing effect could be a result of a rescue of the neurodevelopmental defects themselves, neuronal branching of GABAergic neurons was monitored following GABA treatment. However, supplementation with GABA could not rescue the fine neuronal branching defects observed in *depdc5-/-* larvae (Figures 5F and 5G) thus suggesting that GABA can only *compensate for*, but *not rescue* the neurodevelopmental defects. Further, when the effect of GABA and rapamycin treatment on larval survival was tested, GABA exposure could not rescue the premature death at 2-3 weeks post fertilization (wpf), while rapamycin treatment extended the life span as long as it was supplemented (Figure 5H). This

supports our conclusion that GABA exposure can only partially compensate for the neurodevelopmental defects.

Hence, these results show that while increasing GABA levels could compensate for defective GABAergic branching, it could not rescue the neurodevelopmental defect itself. This also indicates that the premature death is essentially due to perturbation of mTOR signaling (which could be rescued by rapamycin), rather than the GABA network defects. Indeed, rapamycin needed to be continually supplemented, since withdrawal of rapamycin led to gradual death (Figure 5H), reiterating the contribution of mTOR deregulation to premature death.

In order to understand if the compensating effect of GABA was mediated through GABA receptors or independently of them, muscimol (a $GABA_A$ receptor agonist), baclofen (a $GABA_B$ receptor agonist) and vigabatrin (an inhibitor of GABA transaminase which increases local GABA concentration) were tested for their effect on *depdc5-/-* larvae (Figure 6A). Interestingly, treatment with the GABA receptor agonists, muscimol, baclofen, and even both in combination could not rescue the hypoactivity. However, exposure to vigabatrin, which increases endogenous GABA level by inhibiting its metabolism, completely rescued the hypoactivity of *depdc5-/-* larvae as well as PTZ hypersensitivity (Figure 6B). This proves that GABA acts through receptor-independent mechanisms in a paracrine fashion. Moreover, the fact that inhibiting GABA metabolism using vigabatrin is sufficient to rescue the phenotype suggests that GABA itself mediates the compensating effects rather than metabolites of GABA.

Altogether these results support the idea that DEPDC5 loss-of-function impairs early neurodevelopment especially GABA network fine branching which is likely to contribute to epileptogenesis, and that mTOR-dependent metabolic changes are more generalized and severe, eventually resulting in premature death.

mTOR-dependent and independent pathways are perturbed in *depdc5-/-* larvae

In order to further understand whether these two phenomena: upregulation of mTOR signaling, and defective development of GABAergic networks are related and act together in the same pathway, or are controlled independently by DEPDC5, the *depdc5-/-* differentially expressed gene dataset was compared to datasets from three other zebrafish models of epilepsy. These included: (1) a *gabra1-/-* zebrafish line recapitulating idiopathic generalized epilepsy, in which GABAergic network is defective (Samarut et al., under review) (2) an mTORopathy epilepsy (*tsc2-/-*) zebrafish model in which mTORC1 activity is increased [20], and (3) a Dravet syndrome zebrafish model (*scn1Lab* mutant carrying a mutation in $Na_v1.1$ [21]), as a neutral mTOR- and GABA-non-related epilepsy model (Figure 6C).

177 genes were found to overlap between the *depdc5* and *gabra1* datasets (15% and 40% of the total number of genes in the *depdc5* and *gabra1* datasets respectively), and remarkably, 99% of them (175/177) showed the same trend of up- or downregulation in both datasets suggesting specific common mechanisms. When functional clustering and annotation of the common genes was performed, these genes were found to be involved in electron transport, embryonic morphogenesis, GABA receptor activity, synapse formation, general synaptic activity, axonogenesis, nucleotide binding and transcription (Figure 6D and Table S3). Interestingly, many factors which have been associated with epilepsy earlier were also dysregulated. This significant overlap between *depdc5* and *gabra1* datasets provides further evidence that DEPDC5 loss-of-function induces broad defects in GABA network.

Since both DEPDC5 and TSC2 are involved in the negative regulation of mTOR, common genes between these two datasets showed mTOR-related pathways as the largest group

of genes, upon functional clustering and annotation (Table S4). About 15% genes of the two datasets were found to be genes encoding for mTOR related members like aminoacyl-tRNA synthetases, stress response and protein phosphorylation. The overlap of the *depdc5* dataset with data from other models of epilepsy (*Scn1Lab*) and autism spectrum disorder (unpublished, data not shown) did not show a significant overlap (only 23 genes in common between *depdc5*-/- and *Scn1Lab*-/- datasets) thus confirming the specificity of the overlaps described above.

Surprisingly, among the 177 common genes between the *gabra1* and *depdc5* datasets which were involved in neurogenesis and GABA networks, only 18 genes were found to be common with the *tsc2* dataset. The non-overlapping nature of 90% (159 of 177) of the genes indicates that these neurodevelopment-associated genes are more likely to be unrelated to mTOR, but rather controlled by DEPDC5 independently of its canonical mTOR-inhibitory function. These observations show that in the absence of DEPDC5, there are mTOR-dependent metabolic changes (which overlap with the *tsc2* model) but also mTOR-independent neurodevelopment defects especially in the GABAergic network (which overlap with the *gabra1* model), a combination of which presumably leads to epilepsy.

Neurodevelopmental defects in *depdc5*-/- larvae are independent of mTOR signaling

In order to confirm the independent nature of the mTOR and GABA pathways, mTOR signaling was assessed following treatment with GABA in *depdc5*+/+ and -/- larvae (Figure 7A). Consistent with the hypothesis, GABA treatment could not rescue the increase in mTOR activity in *depdc5*-/- larvae (Figure 7A, upper panel). Moreover, the levels of phospho-S6 were also checked in *gabra1*-/- larvae, which have defective GABA signaling and it did not show any

297 change (Figure 7A lower panel). These results indicate that GABA and its related metabolism do
298 not control mTOR signaling.

299 Further, in order to confirm that the neurodevelopmental defects induced by *depdc5* loss-
300 of-function are indeed mTOR-independent, the ability of rapamycin to rescue the fine branching
301 of the GABAergic network in *depdc5-/-* larval brains was assessed. Brain slices from rapamycin
302 treated *depdc5*+/+ and -/- larvae were immunostained using α-GAD65/67. Rapamycin treatment
303 failed to rescue the reduced fine branching of the GABAergic network during development in
304 *depdc5-/-*. Indeed, similar to what was observed in untreated *depdc5-/-* brains (Figure 4), the
305 GAD65/67-positive neurofilaments were less arborized even after rapamycin treatment (Figure
306 7B and 7C), proving that the GABAergic branching defects resulting from the absence of
307 DEPDC5 are indeed mTOR-independent. Of note, phospho-S6 levels are significantly reduced
308 when rapamycin was applied at this concentration (Figure 7D).

309 To confirm the mTOR-independent effects at the molecular level, the ability of
310 rapamycin to restore the expression of critical up- and downregulated genes back to normal was
311 tested in order to assess if the transcriptional changes were also mTOR independent. The genes
312 that were chosen for testing by RT-qPCR were related to axon guidance (*plxn2a, sema3b,*
313 *efnb3b*) and GABA synapse (*gabrg2, gat3, kcc2*), which were in common with the *gabra1*
314 dataset, and also some mitochondrial factors (*mt-cyb, mt-co2*). Consistently with their
315 involvement in metabolic processes, the expression of mitochondrial cytochrome B and
316 cytochrome C oxidase II genes in *depdc5-/-* brains was decreased to wild-type level upon
317 rapamycin treatment (Figure 7E). However, for the genes involved in axon guidance and GABA
318 synapse activity, rapamycin treatment could not rescue the reduced expression observed in
319 *depdc5-/-* larval brains (Figure 7E). This incapability of rapamycin to rescue both, the

neurodevelopmental defects and the transcriptional changes proves that the molecular defects are indeed mTOR-independent.

Lastly, if GABAergic network defects induced by *DEPDC5* knockout are mTOR independent, GABA would not have any effect on another genetic model of mTOR hyperactivation such as *tsc2-/-* [20]. Consistently, when tested on *tsc2-/-* larvae, GABA was unable to rescue the hypoactivity, again validating the mTOR-independent nature of the defects observed in *depdc5-/-* larvae (Figure 7F). Of note, rapamycin, which was used as a positive control could rescue the hypoactivity observed in *tsc2-/-* larvae.

Hence, these results show that at the phenotypic, cellular and molecular levels, alongside its canonical mTOR inhibitory function, DEPDC5 does control neurodevelopmental aspects of GABAergic networks in an mTOR independent fashion.

Discussion:

Mutations in the members of the mTOR-inhibitory GATOR1 complex have recently been shown to be associated with focal epilepsy [7-10]. However, multiple aspects of this complex remain poorly understood, including the molecular pathways through which it plays a role in normal brain activity and/or development.

Depdc5 is strongly expressed in the developing vertebrate nervous system as shown by *in situ* hybridization of early zebrafish embryos, indicating a role for this protein in neuronal development. DEPDC5 is expressed specifically in neurons in the human brain (Human protein atlas database and Human brain transcriptome project) where the transcript was first identified [2, 22], but this is the first report showing its strong expression in the developing vertebrate neural system.

In order to understand the role of DEPDC5 in neurodevelopment and brain activity, the first zebrafish knockout model of *depdc5* was generated and studied. Although rodent models have been recently generated [14-16], the zebrafish model proffers specific technical advantages for studying early neurodevelopment. Though *depdc5-/-* zebrafish larvae do not show obvious phenotypic changes, they exhibit transient spontaneous epileptiform discharges in their brain and increased seizure susceptibility before they die prematurely at about 2 wpf. The zebrafish model also proffers a platform for drug screening purposes. Our zebrafish model would be convenient for initial high-throughput drug screening assays that could identify candidate molecules restoring *depdc5-/-* larval phenotype (i.e. hypoactivity and seizure susceptibility) and later be confirmed in mammalian models. Such an approach using complementary vertebrate models has proven to be effective and time-saving in identifying new therapeutics for other genetic diseases [23].

Hypoactivity and seizure susceptibility of the larvae was consistently observed and could be used as an accurate readout for further studies. It is noteworthy that another zebrafish model with hyperactive mTOR owing to mutated *tsc2* also shows hypoactivity and premature death along with epileptic seizures [20]. Also, since the hypoactivity is observed from very early on, coiling could also be used as a readout in drug screening to economize on time. Notably, no enlarged or abnormal cells were detected in the developing zebrafish brains in this model. This could be explained by the "two-hit" hypothesis where an additional hit along with *DEPDC5* mutations occurs to cause FCD in patients [9]. Also, though *depdc5-/-* larvae show considerably less mRNA levels, it was not completely absent, probably due to incomplete degradation of *depdc5* mRNA by nonsense-mediated decay. However, the significant reduction of mRNA levels show that the phenotypes observed were a result of haploinsufficiency.

With the aim to get further insights into the molecular perturbations in the epileptic *depdc5*-/- brains, transcriptomic analysis was performed in this study, which showed interesting candidates that were up- or downregulated. This is the first report of an *in vivo* transcriptomic profile from a model of dysfunctional GATOR1 complex. As expected, various mTOR-regulated pathways like amino acid metabolism were upregulated owing to mTOR deregulation, including most amino acyl tRNA synthetases. While loss-of-function mutations in some aminoacyl-tRNA synthetases have been shown to be associated with epilepsy [24-27], the contribution of such a broad upregulation in expression levels of these factors to epilepsy remains to be understood.

Interestingly, though factors associated with neurogenesis, axonogenesis and synaptic functions were downregulated, rather than gross morphological defect or neuron loss, specific downregulation of GABA receptors, transporters and factors involved in inhibitory network development, synapse formation and function was observed, revealing for the first time the possible role of DEPDC5 in the formation, pruning and maintenance of the GABAergic system.

GABA exposure could partially compensate the phenotype observed in *depdc5*-/- larvae. The use of GABA receptor agonists in mTORopathies has been explored only for TSC [28], but muscimol and baclofen were ineffective in *depdc5*-/- larvae. These observations suggest that the compensating effect of GABA is more likely to be a paracrine effect of GABA rather than through GABA receptors. In this context, the ability of vigabatrin to rescue the phenotype also confirms the direct effect of GABA rather than of its metabolites. Notably, GABA can only partially ameliorate the *depdc5*-/- phenotype and therefore cannot be considered as a candidate drug against refractory epilepsies. However, the observation that GABAergic networks are affected early during development in a vertebrate *DEPDC5* knockout model is an important consideration for treatment strategies. Indeed, it might be useful to design therapeutic strategies

that can restore or at least compensate stably, the neurodevelopmental defects, rather than solely trying to treat symptomatically, i.e., alleviate the seizures. Notably, the paracrine effect of GABA observed here is also significant since many patients with mutations in *DEPDC5* are refractory to conventional anti-epileptic drugs, which generally act through GABA receptors such as benzodiazepines. Thus, the application of molecules that would increase GABA signaling independently of GABA receptors (such as vigabatrin) could be interesting in the context of these refractory epilepsies.

Predictably, rapamycin could rescue the phenotype, and also prevent premature death, suggesting that mTOR deregulation affects multiple organismal functions. Rapamycin and rapalogs have proved to be extremely effective against many mTOR associated diseases including cancer, lymphangioleiomyomatosis (LAM) and tuberous sclerosis [29-31]. Rapamycin has also been shown to extend longevity and have neuroprotective effects [32, 33]. Like in earlier studies with other diseases, though very effective, cessation of rapamycin treatment led to reappearance of the symptoms and death [30, 34]. Due to various reasons including activation of alternate or compensatory pathways, rapamycin treatment has had modest outcomes in clinical trials despite very promising pre-clinical animal model studies [35]. Hence, rapamycin and rapalogs are now being tested for combination therapy as chemotherapeutic agents, and these could also be applied to treat focal epilepsies, since there is a need to identify new targetable mechanisms of focal epilepsy in order to design new drugs against refractory seizures.

Through multiple comparison of transcriptomic datasets, a large set of genes from the *depdc5* dataset was found to overlap with the *gabra1* dataset independently of the *tsc2* dataset, suggesting that DEPDC5 has unexpected mTOR-independent activity, especially in regulating GABA network development, as proven experimentally (Figure 7). Hence, it is possible that the

two inhibitory complexes, GATOR1 (via DEPDC5) and TSC play distinct roles in different pathways and cell types in addition to their overlapping mTOR-related functions. DEPDC5 function is still incompletely understood and many epileptic mutations have been identified in different domains of DEPDC5 including DUF3608 [2, 3], which also supports the idea that there could be other yet undiscovered functions of DEPDC5. Though mTOR activity has been associated with proper neuronal development [36-38], this study shows that the neurodevelopmental role of DEPDC5 is mTOR-independent. Hence, in addition to controlling neuronal development through mTOR, the components of the pathway might also have mTOR-independent roles.

Altogether, these results show a novel mTOR-independent effect of DEPDC5 on the GABAergic network that is very likely to be a key component of DEPDC5-mediated focal epilepsy substratum. Indeed, abnormal wiring and functioning of the GABAergic system have been observed in epilepsy [39] and GABA agonists have been used for decades alongside other drugs like sodium and calcium channel blockers, glutamate blockers, carbonic anhydrase inhibitors, and other drugs as anti-epileptics [40, 41]. Since GABA is the primary inhibitory neurotransmitter in the cortex, GABA agonists have long been considered the logical choice as anti-epileptic agents. However, in the emerging field of epilepsies caused by mutations in non-ion channel genes, the contribution of the GABAergic network to epilepsy has not been studied and this study shows that modulation of the GABAergic network together with targeting mTOR could be very effective against this class of non-ion channelopathies.

Acknowledgements:

We thank Dr. Louis-Charles Levros and Prof. Patrick Cossette for useful discussions regarding the GABA agonists, Florent Guilloteau and Patrick Gendron from the IRIC genomic platform for discussions regarding the RNA-sequencing experiment, Marina Drits for assistance with fish maintenance. We thank Dr. Kessen Patten and Prof. Jacques Samarut for critical reading and valuable comments on the manuscript. This work was funded by The Savoy Foundation, the Fonds de Recherche Québec Santé (FRQS), the Rare Disease Model and Mechanism network, Dravet Canada, FRQS-affiliated GRSNC (Groupe de Recherche sur le Système Nerveux Central), the Québec MEESR (Ministère de l'Éducation, de l'Enseignement Supérieur et de Recherche), the CRCHUM and the Agence Nationale pour la Recherche (ANR) (grant ANR-16-CE18-0010 to N.S.Y.).

Author contributions:

The project was conceptualized by ES and PD. ES generated and characterized the CRISPR line with assistance from ML and RR. AS and ES performed most of the experiments. AlS and PAMW performed the analyzed the brain epileptiform activity. NSY designed and analyzed the immunolabeling experiment, which RHA and SR performed. AS and ES wrote the manuscript, which was edited by PD.

Declaration of interests: The authors declare no competing interests.

References:

1. Baulac, S. (2014). Genetics advances in autosomal dominant focal epilepsies: focus on DEPDC5. Prog Brain Res *213*, 123-139.

2. Dibbens, L.M., de Vries, B., Donatello, S., Heron, S.E., Hodgson, B.L., Chintawar, S., Crompton, D.E., Hughes, J.N., Bellows, S.T., Klein, K.M., et al. (2013). Mutations in DEPDC5 cause familial focal epilepsy with variable foci. Nat Genet *45*, 546-551.
3. Ishida, S., Picard, F., Rudolf, G., Noe, E., Achaz, G., Thomas, P., Genton, P., Mundwiller, E., Wolff, M., Marescaux, C., et al. (2013). Mutations of DEPDC5 cause autosomal dominant focal epilepsies. Nat Genet *45*, 552-555.
4. Xiong, L., Labuda, M., Li, D.S., Hudson, T.J., Desbiens, R., Patry, G., Verret, S., Langevin, P., Mercho, S., Seni, M.H., et al. (1999). Mapping of a gene determining familial partial epilepsy with variable foci to chromosome 22q11-q12. Am J Hum Genet *65*, 1698-1710.
5. Picard, F., Makrythanasis, P., Navarro, V., Ishida, S., de Bellescize, J., Ville, D., Weckhuysen, S., Fosselle, E., Suls, A., De Jonghe, P., et al. (2014). DEPDC5 mutations in families presenting as autosomal dominant nocturnal frontal lobe epilepsy. Neurology *82*, 2101-2106.
6. Bar-Peled, L., Chantranupong, L., Cherniack, A.D., Chen, W.W., Ottina, K.A., Grabiner, B.C., Spear, E.D., Carter, S.L., Meyerson, M., and Sabatini, D.M. (2013). A Tumor suppressor complex with GAP activity for the Rag GTPases that signal amino acid sufficiency to mTORC1. Science *340*, 1100-1106.
7. Ricos, M.G., Hodgson, B.L., Pippucci, T., Saidin, A., Ong, Y.S., Heron, S.E., Licchetta, L., Bisulli, F., Bayly, M.A., Hughes, J., et al. (2016). Mutations in the mammalian target of rapamycin pathway regulators NPRL2 and NPRL3 cause focal epilepsy. Ann Neurol *79*, 120-131.
8. Scheffer, I.E., Heron, S.E., Regan, B.M., Mandelstam, S., Crompton, D.E., Hodgson, B.L., Licchetta, L., Provini, F., Bisulli, F., Vadlamudi, L., et al. (2014). Mutations in mammalian target of rapamycin regulator DEPDC5 cause focal epilepsy with brain malformations. Ann Neurol *75*, 782-787.
9. Baulac, S., Ishida, S., Marsan, E., Miquel, C., Biraben, A., Nguyen, D.K., Nordli, D., Cossette, P., Nguyen, S., Lambrecq, V., et al. (2015). Familial focal epilepsy with focal cortical dysplasia due to DEPDC5 mutations. Ann Neurol *77*, 675-683.
10. D'Gama, A.M., Geng, Y., Couto, J.A., Martin, B., Boyle, E.A., LaCoursiere, C.M., Hossain, A., Hatem, N.E., Barry, B.J., Kwiatkowski, D.J., et al. (2015). Mammalian target of rapamycin pathway mutations cause hemimegalencephaly and focal cortical dysplasia. Ann Neurol *77*, 720-725.
11. Crino, P.B. (2016). The mTOR signalling cascade: paving new roads to cure neurological disease. Nat Rev Neurol *12*, 379-392.
12. Ostendorf, A.P., and Wong, M. (2015). mTOR inhibition in epilepsy: rationale and clinical perspectives. CNS Drugs *29*, 91-99.
13. Palavra, F., Robalo, C., and Reis, F. (2017). Recent Advances and Challenges of mTOR Inhibitors Use in the Treatment of Patients with Tuberous Sclerosis Complex. Oxid Med Cell Longev *2017*, 9820181.
14. Marsan, E., Ishida, S., Schramm, A., Weckhuysen, S., Muraca, G., Lecas, S., Liang, N., Treins, C., Pende, M., Roussel, D., et al. (2016). Depdc5 knockout rat: A novel model of mTORopathy. Neurobiol Dis *89*, 180-189.
15. Hughes, J., Dawson, R., Tea, M., McAninch, D., Piltz, S., Jackson, D., Stewart, L., Ricos, M.G., Dibbens, L.M., Harvey, N.L., et al. (2017). Knockout of the epilepsy gene Depdc5 in

mice causes severe embryonic dysmorphology with hyperactivity of mTORC1 signalling. Sci Rep *7*, 12618.

16. Yuskaitis, C.J., Jones, B.M., Wolfson, R.L., Super, C.E., Dhamne, S.C., Rotenberg, A., Sabatini, D.M., Sahin, M., and Poduri, A. (2017). A mouse model of DEPDC5-related epilepsy: Neuronal loss of Depdc5 causes dysplastic and ectopic neurons, increased mTOR signaling, and seizure susceptibility. Neurobiol Dis *111*, 91-101.
17. Martin, C., Meloche, C., Rioux, M.F., Nguyen, D.K., Carmant, L., Andermann, E., Gravel, M., and Cossette, P. (2014). A recurrent mutation in DEPDC5 predisposes to focal epilepsies in the French-Canadian population. Clin Genet *86*, 570-574.
18. Hay, N., and Sonenberg, N. (2004). Upstream and downstream of mTOR. Genes Dev *18*, 1926-1945.
19. Zdebik, A.A., Mahmood, F., Stanescu, H.C., Kleta, R., Bockenhauer, D., and Russell, C. (2013). Epilepsy in kcnj10 morphant zebrafish assessed with a novel method for long-term EEG recordings. PLoS One *8*, e79765.
20. Scheldeman, C., Mills, J.D., Siekierska, A., Serra, I., Copmans, D., Iyer, A.M., Whalley, B.J., Maes, J., Jansen, A.C., Lagae, L., et al. (2017). mTOR-related neuropathology in mutant tsc2 zebrafish: Phenotypic, transcriptomic and pharmacological analysis. Neurobiol Dis *108*, 225-237.
21. Baraban, S.C., Dinday, M.T., and Hortopan, G.A. (2013). Drug screening in Scn1a zebrafish mutant identifies clemizole as a potential Dravet syndrome treatment. Nat Commun *4*, 2410.
22. Ishikawa, K., Nagase, T., Suyama, M., Miyajima, N., Tanaka, A., Kotani, H., Nomura, N., and Ohara, O. (1998). Prediction of the coding sequences of unidentified human genes. X. The complete sequences of 100 new cDNA clones from brain which can code for large proteins in vitro. DNA Res *5*, 169-176.
23. Patten, S.A., Aggad, D., Martinez, J., Tremblay, E., Petrillo, J., Armstrong, G.A., La Fontaine, A., Maios, C., Liao, M., Ciura, S., et al. (2017). Neuroleptics as therapeutic compounds stabilizing neuromuscular transmission in amyotrophic lateral sclerosis. JCI Insight *2*.
24. Almalki, A., Alston, C.L., Parker, A., Simonic, I., Mehta, S.G., He, L., Reza, M., Oliveira, J.M., Lightowlers, R.N., McFarland, R., et al. (2014). Mutation of the human mitochondrial phenylalanine-tRNA synthetase causes infantile-onset epilepsy and cytochrome c oxidase deficiency. Biochim Biophys Acta *1842*, 56-64.
25. Zhang, X., Ling, J., Barcia, G., Jing, L., Wu, J., Barry, B.J., Mochida, G.H., Hill, R.S., Weimer, J.M., Stein, Q., et al. (2014). Mutations in QARS, encoding glutaminyl-tRNA synthetase, cause progressive microcephaly, cerebral-cerebellar atrophy, and intractable seizures. Am J Hum Genet *94*, 547-558.
26. Hallmann, K., Zsurka, G., Moskau-Hartmann, S., Kirschner, J., Korinthenberg, R., Ruppert, A.K., Ozdemir, O., Weber, Y., Becker, F., Lerche, H., et al. (2014). A homozygous splice-site mutation in CARS2 is associated with progressive myoclonic epilepsy. Neurology *83*, 2183-2187.
27. Nishri, D., Goldberg-Stern, H., Noyman, I., Blumkin, L., Kivity, S., Saitsu, H., Nakashima, M., Matsumoto, N., Leshinsky-Silver, E., Lerman-Sagie, T., et al. (2016). RARS2 mutations

cause early onset epileptic encephalopathy without ponto-cerebellar hypoplasia. Eur J Paediatr Neurol *20*, 412-417.

28. Curatolo, P., Verdecchia, M., and Bombardieri, R. (2001). Vigabatrin for tuberous sclerosis complex. Brain Dev *23*, 649-653.

29. Wander, S.A., Hennessy, B.T., and Slingerland, J.M. (2011). Next-generation mTOR inhibitors in clinical oncology: how pathway complexity informs therapeutic strategy. J Clin Invest *121*, 1231-1241.

30. Bissler, J.J., McCormack, F.X., Young, L.R., Elwing, J.M., Chuck, G., Leonard, J.M., Schmithorst, V.J., Laor, T., Brody, A.S., Bean, J., et al. (2008). Sirolimus for angiomyolipoma in tuberous sclerosis complex or lymphangioleiomyomatosis. N Engl J Med *358*, 140-151.

31. Muncy, J., Butler, I.J., and Koenig, M.K. (2009). Rapamycin reduces seizure frequency in tuberous sclerosis complex. J Child Neurol *24*, 477.

32. Bové, J., Martínez-Vicente, M., and Vila, M. (2011). Fighting neurodegeneration with rapamycin: mechanistic insights. Nat Rev Neurosci *12*, 437-452.

33. Harrison, D.E., Strong, R., Sharp, Z.D., Nelson, J.F., Astle, C.M., Flurkey, K., Nadon, N.L., Wilkinson, J.E., Frenkel, K., Carter, C.S., et al. (2009). Rapamycin fed late in life extends lifespan in genetically heterogeneous mice. Nature *460*, 392-395.

34. McCormack, F.X., Inoue, Y., Moss, J., Singer, L.G., Strange, C., Nakata, K., Barker, A.F., Chapman, J.T., Brantly, M.L., Stocks, J.M., et al. (2011). Efficacy and safety of sirolimus in lymphangioleiomyomatosis. N Engl J Med *364*, 1595-1606.

35. Li, J., Kim, S.G., and Blenis, J. (2014). Rapamycin: one drug, many effects. Cell Metab *19*, 373-379.

36. Fu, C., Cawthon, B., Clinkscales, W., Bruce, A., Winzenburger, P., and Ess, K.C. (2012). GABAergic interneuron development and function is modulated by the Tsc1 gene. Cereb Cortex *22*, 2111-2119.

37. Westerholz, S., de Lima, A.D., and Voigt, T. (2013). Thyroid hormone-dependent development of early cortical networks: temporal specificity and the contribution of trkB and mTOR pathways. Front Cell Neurosci *7*, 121.

38. Garza-Lombó, C., and Gonsebatt, M.E. (2016). Mammalian Target of Rapamycin: Its Role in Early Neural Development and in Adult and Aged Brain Function. Front Cell Neurosci *10*, 157.

39. Treiman, D.M. (2001). GABAergic mechanisms in epilepsy. Epilepsia *42 Suppl 3*, 8-12.

40. Ashton, H., and Young, A.H. (2003). GABA-ergic drugs: exit stage left, enter stage right. J Psychopharmacol *17*, 174-178.

41. Jembrek, M.J., and Vlainic, J. (2015). GABA Receptors: Pharmacological Potential and Pitfalls. Curr Pharm Des *21*, 4943-4959.

42. Moreno-Mateos, M.A., Vejnar, C.E., Beaudoin, J.D., Fernandez, J.P., Mis, E.K., Khokha, M.K., and Giraldez, A.J. (2015). CRISPRscan: designing highly efficient sgRNAs for CRISPR-Cas9 targeting in vivo. Nat Methods *12*, 982-988.

43. Thisse, C., and Thisse, B. (2008). High-resolution in situ hybridization to whole-mount zebrafish embryos. Nat Protoc *3*, 59-69.

44. Huang da, W., Sherman, B.T., and Lempicki, R.A. (2009). Systematic and integrative analysis of large gene lists using DAVID bioinformatics resources. Nature Protocols *4*, 44-57.
45. Puverel, S., Nakatani, H., Parras, C., and Soussi-Yanicostas, N. (2009). Prokineticin receptor 2 expression identifies migrating neuroblasts and their subventricular zone transient-amplifying progenitors in adult mice. J Comp Neurol *512*, 232-242.

Figure legends:

Figure 1: *depdc5* is essential for survival. (A) Whole mount *in situ* hybridization showing expression of *depdc5* at different stages of development. (B) Electropherograms showing confirmation of the 4 bp insertion by Sanger sequencing. (C) Expression of *depdc5* transcript in 7 dpf *depdc5*+/+, +/- and -/- larvae (N=3, Student's t test: p (WT vs HT)=0.0026; p (WT vs HM)=0.001). (D) Survival curve showing that *depdc5-/-* embryos have reduced survival with most larvae dying around 14 dpf (N=2, n=15 per genotype). (E) Images showing that *depdc5*-/- larvae don't show gross morphological changes at 3 dpf. (F) Measurement of body length (upper panel; n=20/genotype; p=0.0045 by unpaired Student's t-test) and eye size (lower panel; n=12/genotype; p=0.7219 by unpaired Student's t-test) showed no significant change in either parameter.

Figure 2: *depdc5* knockout results in increased mTOR activity, hypoactivity, epileptiform discharges and seizure susceptibility. (A) Western blotting of 7 dpf larval lysates to examine phospho-S6 levels in *depdc5*+/+, *depdc5*+/- and *depdc5*-/- larvae showing hyperactivation of mTOR signalling. (n=3; p(WTvsHT) = 0.0012; p(WTvsHM) = 0.0455). (B) Images of 6 dpf *depdc5*+/+ and *depdc5*-/- larval brains (transversal sections across the optic tectum) immunostained with phospho-S6 antibodies and counterstained with DAPI. The panels on the extreme right depict 3D reconstruction of single cells in *depdc5*+/+ and -/- brains (Scale bars

from left to right panels: 20µm, 2.5µm, 1.5µm). (C) Spontaneous extracellular electrographic activity recorded from the optic tectum of *depdc5*+/+ or *depdc5*-/- larvae at 9 dpf showing representative epileptiform activity of *depdc5*-/- larvae displaying polyspiking discharges. (D) Percentage of *depdc5*+/+ and *depdc5*-/- larvae showing epileptiform activity in the brain (N=4; n=10/genotype, Student's t-test p(WTvs HM)<0.0001). (E) Distance swam by 8 dpf larvae across two 2 hour dark-4 hour light cycles. (F) Spontaneous coiling activity in 20 hpf embryos monitored over 20 minutes represented as the percentage of total time during which the embryos were active (N=3, n=20, Student's t-test p (WT vs HM)<0.0001). (G) Distance swam by 2 dpf embryos upon exposure to 3mM PTZ represented as fold change compared to basal distance swam by wildtype larvae at t_0. (N=3, n>10, student t-test, *: p<0.05) (H) Representative swimming tracks of 2 dpf embryos during a 10-minute period following a 3mM PTZ exposure (tracks of 3 replicates are shown in rows for each genotype).

Figure 3: *depdc5* knockout alters gene expression in larval brains without affecting brain morphology (A) Volcano plot showing the differentially expressed gene expression profile between *depdc5*+/+ and *depdc5*-/- larval brains. See also Table S1. (B) Pathways showing high enrichment in the differentially expressed genes (upregulated are shown in green, downregulated, in red). (C) Whole mount images of *depdc5*+/+ and -/- larvae at different stages of development immunostained with α-acetylated tubulin. (n>3/genotype/developmental stage; Scale bar:40 µm).(D) Measurement of head size and head surface area in 3 dpf *depdc5*+/+ and *depdc5*-/- larvae. (E) Whole mount images of 48 hpf *depdc5*+/+ and -/- larvae immunostained with α-phosphorylated histone H3 (n>3/genotype). (F) Cresyl violet staining comparing 7 dpf

635 *depdc5*+/+ (top half) and *depdc5*-/- (bottom half) larval heads showed no gross difference in the
636 density of cells in the brain. Scale bar=100 μm.
637
638 **Figure 4: Defects in GABAergic networks in *depdc5* knockout zebrafish brains.** Images of
639 transverse sections of 6 dpf *depdc5*+/+ and *depdc5*-/- embryos immunostained with GAD65/67
640 (A), gephyrin (C) and Nlgn2 (D) antibodies and counterstained with DAPI. Section level is
641 displayed in the schematic drawing. Regions indicated in red boxes have been magnified to show
642 the branching defects (N=3, n=3 embryos/genotype). Scale bar: 10 μm. (B**)** Imaris-reconstructed
643 3D image with Gad65/67 positive GABAergic boutons shown in green projecting towards the
644 nucleus (DAPI) shown in blue. (Scale bar=2 μm). (E) Images of longitudinal sections of 6 dpf
645 *depdc5*+/+ and *depdc5*-/- embryos immunostained with parvalbumin 7 antibody (Scale
646 bar=25μm). Field of view is displayed in the schematic drawing (F) Quantification of the number
647 of GAD65/67-positive neurofilaments, gephyrin-positive puncta and parvalbumin-positive cells
648 in *depdc5*+/+ and -/- larval brain sections (N=3, n>3 embryos/genotype).
649
650 **Figure 5: Rescuing effect of GABA and rapamycin on *depdc5* knockout zebrafish.** (A)
651 Swimming activity of 8 dpf larvae, with the activity of *depdc5* +/+ larvae normalized to 100%
652 shows that treatment with GABA (100 μM) can completely rescue hypoactivity (N=2,
653 n=20/genotype/treatment). Rapamycin treatment (100 nM from day 0-2, 300 nM from day 3
654 onwards) was used as a positive control. (B) Spontaneous coiling activity in 20 hpf embryos
655 shows that the hypoactivity of *depdc5*-/- embryos is rescued by treating with 100 nM rapamycin
656 or with 100 μM GABA from single-cell stage (N=2, n=20/genotype/treatment, Student's t-test p
657 (Control WT vs HM) <0.0001:****). Coiling activity of *depdc5*+/+ was set at 100% for each

sample, and the relative activity of the *depdc5-/-* larvae is represented. (C) Western blotting of 9 dpf larval lysates to examine phospho-S6 levels in *depdc5+/+* and *depdc5-/-* larvae treated with DMSO or rapamycin (100 nM from day 0-2, 300 nM from day 3 onwards) shows inhibition of mTOR signaling upon rapamycin treatment. (D) Distance swam by 2 dpf larvae treated with GABA (100μM) or rapamycin (100nM) upon PTZ exposure (3mM) (N=3, n>10). (E) Representative swimming tracks of 2 dpf embryos (untreated or treated with GABA or rapamycin) during a 10-minute period following PTZ exposure (3mM). (F) Images of transverse sections of 7 dpf GABA treated *depdc5+/+* and *depc5-/-* larval brains immunostained with α-GAD65/67 and counterstained with DAPI. Regions indicated in red boxes have been magnified to show the branching defects. GABA treatment (100 μM) was begun at 8 hpf (n=3 embryos/genotype). (G) Quantification of the number of GAD65/67 positive neurofilaments in GABA-treated *depdc5+/+* and -/- larval brain sections showing that GABA treatment does not rescue the defects in *depdc5-/-*. (H) Survival curve showing that treatment of *depdc5-/-* larvae with rapamycin (100 nM from day 0-2, 300 nM from day 3 onwards) first prolongs lifespan as long as rapamycin is supplemented to the water (till day 20-shaded). Withdrawal of rapamycin results in a drop in survival and all the larvae die by day 35. On the contrary, treatment with 100 μM GABA from 8 hpf doesn't extend survival. Both rapamycin and GABA did not affect *depdc5+/+*.

Figure 6: Paracrine compensation by GABA and modulation of multiple independent pathways in *depdc5* knockout zebrafish. (A) Swimming activity of 8 dpf larvae treated with muscimol (100 μM), baclofen (100 μM), a combination of both or vigabatrin (5 mM) with the activity of *depdc5+/+* larvae normalized to 100% shows that treatment with vigabatrin can

completely rescue hypoactivity, while GABA receptor agonists cannot. (B) Vigabatrin treatment completely rescues PTZ-hypersensitivity of 2 dpf *depdc5*-/- embryos (N=2, n>30; student t-test, *: p value <0.05). (C) Overlap between gene expression datasets from *depdc5*, *gabra1*, *tsc2* and *scn1a* mutants. See also Tables S2 and S4. (D) A representation of the common pathways (axon guidance and GABA synapse) affected in *depdc5* and *gabra1* knockout brains with the common genes indicated. See also Table S3.

Figure 7: mTOR deregulation and GABAergic defects are independent effects of Depdc5 knockout. (A) Western blotting of 7 dpf *depdc5*+/+ and *depdc5*-/- larval lysates shows no change in phospho-S6 levels upon GABA treatment (100 μM from 8 hpf; top panel). Western blotting of 7 dpf *gabra1*+/+ and *gabra1*-/- larval lysates shows no difference in mTOR signaling upon knocking out *gabra1* (bottom panel). (B) Images of transverse sections of 7 dpf rapamycin treated *depdc5*+/+ and *depc5*-/- larvae immunostained with α-GAD65/67 and counterstained with DAPI. Section level is displayed in the schematic drawing. Regions indicated in red boxes have been magnified to show the branching defects. Rapamycin treatment was begun at 8 hpf: 100 nM from day 0-2, 300 nM from day 3 onwards (n=3/genotype). Scale bar=10 μm. (C) Quantification of GAD65/67 positive neurofilaments in rapamycin treated *depdc5*+/+ and -/- larval brain sections shows that rapamycin treatment does not rescue the reduced number of filaments in *depdc5*-/-. (D) Western blotting of 5 dpf larval lysates upon treatment with increasing concentrations of rapamycin (50 nM, 250 nM, 500 nM, 1 μM and 2.5 μM) from 8 hpf to estimate phospho-S6 levels shows a dose-dependent decrease. Rapamycin-containing water was changed everyday. (E) qRT-PCR based estimation of some down- and upregulated genes involved in axon guidance, GABA synapse and metabolism. *ef1a* expression was used for

normalization, expression of *depdc5*+/+ was normalized to 1. ($p<0.05$:*; $p<0.01$:**). (F) Swimming activity of 7 dpf *tsc2* larvae treated with rapamycin and GABA (day 0 onwards) over 5 minute light-10 minute dark phases, with the activity of *tsc2*+/+ larvae normalized to 100% shows that rapamycin, but not GABA can rescue the hypoactivity (Student's t-test $p<0.0001$:****).

STAR methods:

Contact for reagent and resource sharing

Further information and requests for resources and reagents should be directed to and will be fulfilled by the Lead contact: Éric Samarut (eric.samarut@umontreal.ca)

Experimental model and subject details

Routine zebrafish (*Danio rerio*) maintenance was performed following standard procedures (Westerfield) at 28.5^0C under 12/12 hour light/dark cycles at the animal facility of the Centre Hospitalier de l'Université de Montréal Research Centre (CRCHUM), Montréal. All experiments were performed in compliance with the guidelines of the Canadian Council for Animal Care. The primary model used for this study was *depdc5* loss of function mutants.

For generation of the *depdc5* loss of function model, zebrafish optimized Cas9 mRNA was synthesized using the mMESSAGE mMACHINE SP6 kit (Ambion) and a pCS2-nCas9n template linearized with NotI. The following gRNA sequence targeting the 14^{th} exon of *depdc5* was designed using the online tool CRISPRscan (PAM site is indicated in brackets): 5'-TGAGGATCATGAGCAAT(CGG)-3'. Synthesis of gRNA and of Cas9 mRNA was performed

as described [42]. Briefly, a 52 nt oligo (sgRNA primer), containing the T7 promoter, the 20 nt of the specific sgRNA DNA binding sequence and a constant 15 nt tail for annealing, was used in combination with a 80 nt reverse oligo to add the sgRNA invariable 3′ end (tail primer). A 117 bp PCR product was generated following these parameters: 3 minutes at 95°C, 30 cycles of 30 seconds at 95°C, 30 seconds at 45°C and 30 seconds at 72°C, and a final step at 72°C for seven minutes. PCR products were purified using Qiaquick (Qiagen) columns and approximately 120–150 ng of DNA were used as template for a T7 In vitro transcription (IVT) reaction (AmpliScribe-T7-Flash transcription kit from Epicentre). In vitro transcribed sgRNAs were DNAse treated and precipitated with Sodium Acetate/Ethanol. Cas9 mRNA was in vitro transcribed from DNA linearized by *XbaI* using the mMachine T3 kit (Ambio). *In vitro* transcribed mRNAs were purified by phenol-chloroform followed by isopropanol precipitation.

Tubingen long fin (TL) wild-type embryos were collected for microinjection. A 1nL drop of a mix of 100 ng/μL of Cas9 mRNA and 30 ng/μL of gRNA was injected into one-cell stage embryos using a Picospritzer III pressure ejector.

Genotyping of *depdc5*+/+ (wild type), +/- (heterozygous) and -/- (homozygous) animals was performed by high resolution melting analysis (HRM) using genomic DNA extracted by boiling the embryo/larva/clipped caudal fin in 50 mM NaOH for 10 minutes and then neutralizing it with 100 mM Tris HCl (pH 8). HRM primers were designed using the Universal Probe Library Assay Design Center (FP: 5’ ATGCGCTGTTTGGTGAGG 3’ and RP: 5’ TCCAGGAGTGGGTGTTTTTG 3’). All primer sets are available upon request. The PCR reactions were made with 5 μL of the Precision Melt Supermix for HRM analysis (Bio-Rad #172-5112), 0.5 μL of each primer (10 μM) and 2 μL of genomic DNA and water up to 10 μL. The PCR was performed in a LightCycler 480 Instrument II (Roche) using white 96 well plates.

Two-step Evagreen PCR reaction protocol was 95°C for 2 min, then 45 cycles of 95°C for 10 sec and 60°C for 30 sec, followed by 95°C for 30 sec, 60°C for 60 sec, the temperature was increased by 0.02°C/sec until 95°C for 10 sec, then cooling at 40°C. Curves were analyzed using the Roche LightCycler 480 software version 1.5.1.62.

In order to eliminate any putative off-target mutations, F0 founder was outcrossed with Tubingen long fin wild-type fish for at least three generations before phenotyping the embryos. All experiments were performed on larvae, and sex of zebrafish is not yet determined at this stage. *depdc5*+/- fish were incrossed to obtain *depdc5*+/+, +/- and -/- from the same cross for experiments. *depdc5*+/- fish of different generations have been used to verify consistency of the phenotype.

Method details

***In situ* hybridization**

A specific probe for *depdc5* corresponding to the 5' part of the coding sequence and first exon (971bp amplified with the following primers: FP: 5' TGACACAGAAAGTAGAGTTTGCAGG 3'; RP: 5' GTTCTCAGCATCTTTGGGAGC 3') was cloned within the pCS2+ vector using TOPO TA cloning kit (Invitrogen). After sequencing, antisense probe was transcribed *in vitro* using SP6 RNA polymerase. Whole-mount *in situ* hybridization of zebrafish embryos was performed as described by Thisse et al., 2008 [43]. Stained embryos were kept in 80% glycerol and imaged.

Western blotting

Larvae were anaesthetized and collected at 8 dpf, following which lysates were rapidly prepared by homogenization in high salt lysis buffer containing 10 mM Tris HCl (pH 8), 20% glycerol,

774 0.4 M KCl, protease and phosphatase inhibitors. After a freeze-thaw cycle to ensure efficient
775 homogenization, the lysates were centrifuged at 13,000 rpm for 20 minutes. The supernatant was
776 collected, and protein concentration was estimated using Bradford assay (Biorad). Western
777 blotting was performed using 30 μg lysate per sample which were resolved on a 12% SDS-
778 polyacrylamide gel. After electrophoresis, proteins on the gel were electrotransferred onto 0.22
779 micron nitrocellulose membrane. The membranes were blocked with 5% non-fat milk solution in
780 1X phosphate buffered saline or with 5% bovine serum albumin (Sigma) in 1X Tris buffered
781 saline for immunoblotting with anti-γ-tubulin (#T6557; Millipore Sigma) or anti-total S6 (2217;
782 Cell Signaling Technologies) and anti-phospho S6 (#2215; Cell Signaling Technologies)
783 respectively. Detection was performed using goat anti-mouse and goat anti-rabbit antibodies
784 respectively conjugated with horse radish peroxidase. Bands were visualized with ECL and
785 imaged using ChemiDoc (Biorad).
786
787 **Non-invasive local field potential (LFP) recordings**
788 Non-invasive recordings reading the electric signal from the head of the larvae were performed
789 based on a modified protocol [19]. The larva was immobilized in 2% low melting point agarose
790 (Invitrogen). Recording electrode (soda lime glass, Hilgenberg, Germany) was pulled with a
791 DMZ Universal Puller (Zeitz, Germany) to a diameter of approximately 20 microns and filled
792 with artificial cerebrospinal fluid (ACSF, 124 mM, NaCl, 2 mM KCl, 2 mM $MgSO_4$, 2 mM
793 $CaCl_2$, 1.25 mM KH_2PO_4, 26 mM $NaHCO_3$ and 10 mM glucose). The differential signal between
794 the recording electrode positioned on larva's head above the optic tectum and the reference
795 electrode was amplified 10,000 times by DAGAN 2400 amplifier (Minnesota, USA), band pass
796 filtered at 0.3-300 Hz and digitized at 2 kHz via a PCI-6251 interface (National Instruments,

UK) with WinEDR (John Dempster, University of Strathclyde, UK). The duration of each recording was 10 minutes. Epileptiform events consisted of multispike bursts with amplitudes exceeding at least three times baseline and lasted for minimum 100 msec. Electrophysiological recordings were analysed using Clampfit 10.2 software (Molecular Devices, USA).

Motor activity measurements

20 hpf embryos were embedded in low melting agarose and their movements inside the chorion were recorded using a camera for 20 minutes during which time they were kept hydrated. The Danioscope software (Noldus) was then used to quantify the percentage of time the embryos were active, the number of bursts and burst duration. At later stages (>5dpf), larvae were transferred individually into a 96-well plate and activity was recorded over light-dark cycles using Basler GenIcam camera and DanioVision recording chamber (Noldus). Analysis was performed using the Ethovision XT 12 software (Noldus) to quantify the distance swam.

Drug treatment

Drugs were procured from Sigma-Aldrich and LC Laboratories and stock solutions were prepared (PTZ-300mM, GABA-100 mM, Muscimol-30 mM, Baclofen-15 mM, Vigabatrin-1M in water and rapamycin-500 μM in DMSO). Embryos were treated from 8 hpf unless mentioned otherwise. The water was replaced everyday with fresh water containing final concentration of the drug, till the activity measurement or end of the survival curve whichever was later. For PTZ assay, manually dechorionated 2 dpf embryos were placed in a 96-well plate and let accommodated for 20-30 minutes. PTZ from stock solution (300mM) was diluted to the final

concentration (3mM) directly in the wells and the embryos were tracked immediately during 20 minutes using a Daniovision (Noldus).

Transcriptomic, differential expression and pathway analyses

Three independent batches of 10 dpf *depdc5*+/+ and -/- larvae were dissected to extract the whole brain, by each of two experimenters, corresponding to experimental triplicates. Total RNA was extracted from these flash frozen brains using PicoPure RNA extraction kit (Thermo Fisher Scientific) following the manufacturer's standard protocol. For each sample, RNA extraction was made from 5 whole brains. Absence of contamination was assessed by Nanodrop using 260/280 and 260/230 ratios. Quality of total RNA was assessed with the BioAnalyzer Nano (Agilent) and all samples had a RIN above 9.

Library preparation was performed using the Truseq RNA (Illumina). 13 PCR cycles were required to amplify cDNA libraries. Libraries were quantified by Nanodrop and BioAnalyzer. All libraries were diluted to 10 nM and normalized with the Miseq SR50 v2. Libraries were pooled to equimolar concentration and multiplexed by 6 samples per lane. Sequencing was performed with the Illumina Hiseq2000 using the SBS Reagent Kit v3 (100 cycles, paired-end) with 1.6 nM of the pooled library. Cluster density was targeted at around 800k clusters/mm^2. Between 45 and 55 million reads were generated for each sample. Library preparation and sequencing was done at the genomics platform of the Institute for Research in Immunology and Cancer (University of Montreal). About 90% of high quality reads were mapped onto the zv9 version of the zebrafish genome (ensemble release 77) using TopHat version 2.0.10.

Differential gene expression analysis was assessed by DeSeq2 package using R software. Genes showing an absolute fold change >1.4 and adjusted p value <0.05 were considered to be

842 significantly differentially expressed. Pathway analysis was performed using DAVID
843 bioinformatics resources [44]. The list of differentially expressed genes was uploaded onto
844 DAVID analysis wizard and a list of all expressed genes found in our dataset was used as a
845 background for gene enrichment analysis.
846
847 **qRT-PCR**
848 400 ng of RNA extracted as described above was used for reverse transcription to prepare cDNA
849 with the Superscript VILO cDNA synthesis kit. The cDNA was diluted 1:10 and used for qPCR
850 with SYBR Green I Master (Roche) on a LightCycler 480 instrument. *ef1a* was used as the
851 reference gene for normalization. Primers were designed using the Roche Universal Library
852 Design Center online tool: gabrg2_F: cattcgtgtcctctcgagttc, gabrg2_R: agctgcgcttccacttgtat;
853 kcc2_F: tggagccatgtacatcttgg, kcc2_R: tggcagctgatggaacaat; gat3_F: tgaacagaacgtgcccatag,
854 gat3_R: cgctataaacgctagaccagga; plxn2a_F: agagcaaaaaccatcccaaa, plxn2a_R:
855 gcatcttctcagcgacagact; sema3b_R: caacatggaccagcaactga, sema3b_R: ccacttgcattcatctcgtc;
856 efnb3b_F: ctacacagggcatgaaggtg, efnb3b_R: ggagatttggctggcaga; mt-cyb_F:
857 tgacttattcggagcatcca, mt-cyb_R: tagtcctcgggcgatgtg; mt-co2_F: gaaattaatgacccccacgttac, mt-
858 co2_R: cgtagcttcagtaccattgatgtc; ef1a_F: gtggctggagacagcaaga, ef1a_R: agagatctgaccagggtggtt.
859
860 **Immunostaining**
861 *depdc5*+/+ and *depdc5*-/- embryos were anaesthetized in 0.2% tricaine, fixed with 4%
862 paraformaldehyde, cryoprotected in 10% sucrose overnight, and embedded in 7.5% gelatin/10%
863 sucrose solution prior to flash freezing in isopentane. Samples were stored at -80°C until use.
864 Embryos were cut into 20-µm-thick sections on cryostat, mounted on superfrost slides, and

stored at −80°C. For gephyrin immunostaining, *depdc5*+/+ and *depdc5*-/- embryos were embedded in OCT and frozen in liquid nitrogen. Cryosections (20 µm) were fixed in 4% paraformaldehyde at room temperature for 10 min. After washing thrice with PBS, sections were treated with 0.25% trypsin in 1X PBS for 2 min at 25°C. Immunohistochemistry was performed as previously described [45]. Briefly, sections were blocked and permeabilized with 0.2% gelatin, 0.25% Triton X100 diluted in 1X PBS for 1 hour at room temperature and then incubated overnight at room temperature with anti-GAD65/67 (1:500, rabbit polyclonal, Ab11070, Abcam), anti-Neuroligin 2 (Nlgn2) (1:300, rabbit polyclonal, Ab 36602, Abcam), or anti-gephyrin (1:100, rabbit polyclonal, ab185930, Abcam). After several washes, sections were incubated for 1 hour with the donkey anti-rabbit coupled to Alexa Fluor 488 (1:500, Jackson Laboratories, West Grove, PA). Sections were counterstained for 10 minutes with 0.1% DAPI (Sigma-Aldrich) before being mounted with Vectashield Mounting Medium (Vector). Sections were analysed using a Leica TCS SP8 confocal scanning system (Leica Microsystems). Eight-bit-digital images were collected using a Leica 40x HCPL APO CS2 oil-immersion objective (numerical aperture 1.30). Full-slices were captured 60-65 z-stacks, with a z step of 0.3 µm. Images were processed with ImageJ software (National Institutes of Health, USA).

For whole mount immunostaining, *depdc5*+/+ and *depdc5*-/- embryos were anaesthetized in 0.2% tricaine, fixed in Dent's fixative (80% methanol and 20% DMSO) overnight. After rehydrating gradually into PBS, the larvae were permeabilized for 7 minutes in cold acetone. Larvae were blocked and permeabilized with 2% normal goat serum, 2% BSA and 1% DMSO diluted in 1X PBS for 1 hour at room temperature and then incubated overnight at 4^0C with anti-acetylated tubulin (1:500, mouse monoclonal, Abcam) or anti-phosphorylated histone H3 (1:500, rabbit polyclonal, Millipore). After several washes, sections were incubated for 2 hours with the

goat anti-rabbit or goat anti-mouse coupled to Alexa Fluor 488. After washing, the fluorescence was analyzed by confocal microscopy (Olympus BX61W1 equipped with a Quorum Technology spinning disk head connected to a Hamamatsu ORCA-ER camera). Images were analysed using Volocity software (Improvision).

Cresyl violet staining

depdc5+/+ and -/- embryos were anaesthetized in 0.2% tricaine, fixed with 10% paraformaldehyde, embedded in paraffin, and sectioned. After deparaffinization and rehydradation, slides were stained with 0.5% cresyl violet (Sigma; in 0.3% acetic acid). Sections were differentiated in 70% ethanol and dehydrated in 100% ethanol. After clearing in xylene, coverslips were mounted using Pertex mounting medium (HistoLab, Gothenburg, Sweden). The slices of embryos were photographed with a microscope Nikon Eclipse (E-200) equipped with a digital sight (Nikon).

Morphological analysis

3 dpf *depdc5*+/+ and -/- larvae were anaesthesized and dorsal and lateral images of the whole body were acquired using the same parameters for all larvae. Body length, eye size, head size and surface area were measured using the Danioscope software. Body length was measured from the anterior tip to the caudal peduncle. Eye size and brain surface area were measured by specifying the eye and brain boundaries.

Quantification and statistical analysis

Quantification of gephyrin-labelled puncta and GAD65/67-labelled neurofilaments

Apotome images from 20 μm sections labelled with anti-gephyrin were deconvoluted using AutoQuant X (version X3.1.1) and processed using Image J (version 1.51s). Z-stacks were manually contrasted to maximize synaptic puncta visibility and reduce background noise. Using a semi-automatic macro, they were segmented by thresholding after filtering only synaptic puncta with diameters varying from 0.15 to 2μm (macro written by Zsolt CSABA, INSERM UMR1141). For each image, the total number of gephyrin-positive synapse puncta was divided by the whole surface filled by these synapses to get the number of synapses per μm^2. The ratios of a total number of images from three independent experiments (n (*depdc5*+/+) =9; n(*depdc5*-/-) =19) were averaged to get the means and standard errors of the means (SEM) and assess statistical tests between the two samples' groups.

For Gad65/67 quantification, 20 μm sections labelled with anti-GAD65/67 were imaged at zoom 6 using Leica HC PL APO CS 40X objective and processed using Bitplane Imaris (version 9.0.2). MeasurementPro's Filaments that detects automatically filament-like structures was used to outline and quantify the dendrites. Images from three independent experiments (n(*depdc5*+/+)=3 ; n(*depdc5*-/-)=3) were used to calculate the means and their standard errors (SEM) and assess statistical tests between the two groups.

Quantification of morphological and locomotion parameters was performed using Danioscope and Ethovision softwares respectively (Noldus) (described above). All data acquisition and quantification was performed by experimenter blind to the genotype of the larva. There is no evident morphological difference between *depdc5*+/+ and -/- which might bias the experimenter. Details of biological and technical replicates, statistical test used and significance are mentioned in the corresponding figure legend. All experiments have been repeated thrice on an average

(represented by N) and the number of animals per genotype used in each experiment is represented by n. In most instances, unpaired Student's t test was performed to estimate statistical significance. If $p>0.05$, not significant, $p\leq0.05$: *, $p\leq0.01$: **, $p\leq0.001$: *** and $p\leq0.0001$:****

Data and software availability

Complete list of significantly up- and downregulated genes ($p<0.05$) in *depdc5-/-* larval brains in comparison to *depdc5*+/+ brains is available in Table S1. Complete list of genes overlapping between the *depdc5* and *gabra1* datasets is available in Table S2. Table S3 has a list of common genes between *depdc5* and *gabra1* datasets classified according to function. Table S4 gives the complete list of genes overlapping between *depdc5* and *tsc2* datasets.

Supplemental file information:

Supplemental videos:

Video S1: 3D GAD65/67-labelled neurofilaments in depdc5+/+ larval brains

Reconstruction of 3D-images from fluorescent immunodetection of GAD65/67 accumulation (green) on cryostat sections of 6 dpf *depdc5*+/+ zebrafish embryos combined with DAPI staining were imaged using confocal microscopy. Subsequently, z-stacks of selected region were rendered into 3D volume using Imaris (Bitplane Inc.).

Related to figure 4.

Video S2: 3D GAD65/67-labelled neurofilaments in depdc5-/- larval brains

Reconstruction of 3D-images from fluorescent immunodetection of GAD65/67 accumulation (green) on cryostat sections of 6 dpf *depdc5*-/- zebrafish embryos combined with DAPI staining were imaged using confocal microscopy. Subsequently, z-stacks of selected region were rendered into 3D volume using Imaris (Bitplane Inc.).

Related to figure 4.

Supplemental tables:

S1 Table: Complete list of significantly up- and downregulated genes in 10 dpf *depdc5*-/- larval brains in comparison to *depdc5*+/+ brains. Description of the top 5 up- and downregulated genes is provided. Related to figure 3.

Table S2: List of common dysregulated genes between *depdc5* and *gabra1* datasets with the fold change and pattern of deregulation. Related to figure 6.

Table S3: Common genes between *depdc5* and *gabra1* datasets classified according to function. Related to figure 6.

Table S4: List of common genes between *depdc5* and *tsc2* datasets. Related to figure 6.

CellPress

KEY RESOURCES TABLE

REAGENT or RESOURCE	SOURCE	IDENTIFIER
Antibodies		
GAD65/67	Abcam	Cat#Ab11070
Gephyrin	Abcam	Cat#Ab185930
Neuroligin 2	Abcam	Cat#Ab36602
Gamma-Tubulin	Millipore Sigma	Cat#T6557
Phospho histone H3	Millipore	Cat#09-838
Phospho ribosomal protein S6	Cell Signaling Technologies	Cat#2215
Ribosomal protein S6	Cell Signaling Technologies	Cat#2217
Acetylated tubulin	Sigma Aldrich	Cat#T7451
Bacterial and Virus Strains		
None	N/A	N/A
Biological Samples		
RNA extracted from 10 dpf larval brains of *depdc5*+/+, +/- and -/-	This manuscript	N/A
Chemicals, Peptides, and Recombinant Proteins		
In situ probe	Synthesized	N/A
Pentylenetetrazol	Sigma	Cat#P6500
Cresyl violet	Sigma	Cat#190-M
Rapamycin	LC Laboratories	Cat#R-5000
GABA	Sigma	Cat#A2129
Vigabatrin	Sigma	Cat#V8261
Muscimol	Sigma	Cat#M1523
Baclofen	Sigma	Cat#B5399
Precision Melt Supermix for High resolution melting (HRM) analysis	Biorad	Cat#172-5112
Critical Commercial Assays		
mMESSAGE mMACHINE SP6 kit	Ambion	Cat#AM1340
TOPO TA cloning kit	Invitrogen	Cat#451641
PicoPure RNA extraction kit	Thermo Fisher Scientific	Cat#KIT0204
Superscript VILO cDNA synthesis kti	Invitrogen	Cat#11754050
Deposited Data		
Tsc2 mutant zebrafish data	[20]	N/A
Gabra1 mutant zebrafish data	Samarut et al (related manuscript, unpublished)	N/A
Depdc5 mutant zebrafish data	This manuscript	N/A
Experimental Models: Cell Lines		
None	N/A	N/A

Experimental Models: Organisms/Strains		
Depdc5 loss of function mutant zebrafish	This manuscript	N/A
Tubingen long fin (TL) wild type zebrafish	ZIRC	ZIRC_ID: ZL86
Oligonucleotides		
Depdc5 HRM primers: sequence in methods	Sigma	N/A
Guide RNA targeting 14th exon of *depdc5* (details of synthesis in methods)	This manuscript	N/A
qPCR primers for *depdc5*, GABA-related, axon-guidance related and metabolism-related genes: sequence in methods	Sigma	N/A
Recombinant DNA		
Plasmid encoding Cas9: pCS2-nCas9n	[42]	N/A
Software and Algorithms		
Danioscope	Noldus	Version 1.1 http://www.noldus.com/danioscope/more-about-danioscope
Ethovision XT	Noldus	XT12 http://www.noldus.com/EthoVision-XT/New
LightCycler 480	Roche	V1.5 https://lifescience.roche.com/en_ca/products/lightcycler14301-480-instrument-ii.html
Image J	NIH	V1.51 https://imagej.nih.gov/ij/download.html
R	The R project	V3.5.0 https://www.r-project.org
Volocity	Improvision-Perkin Elmer	V3 http://cellularimaging.perkinelmer.com/downloads/detail.php?id=14
Imagelab	Biorad	V4.1 http://www.bio-rad.com/en-ca/product/image-lab-software?ID=KRE6P5E8Z
Other		

Figure 1

Click here to download Figure Fig 1.tif

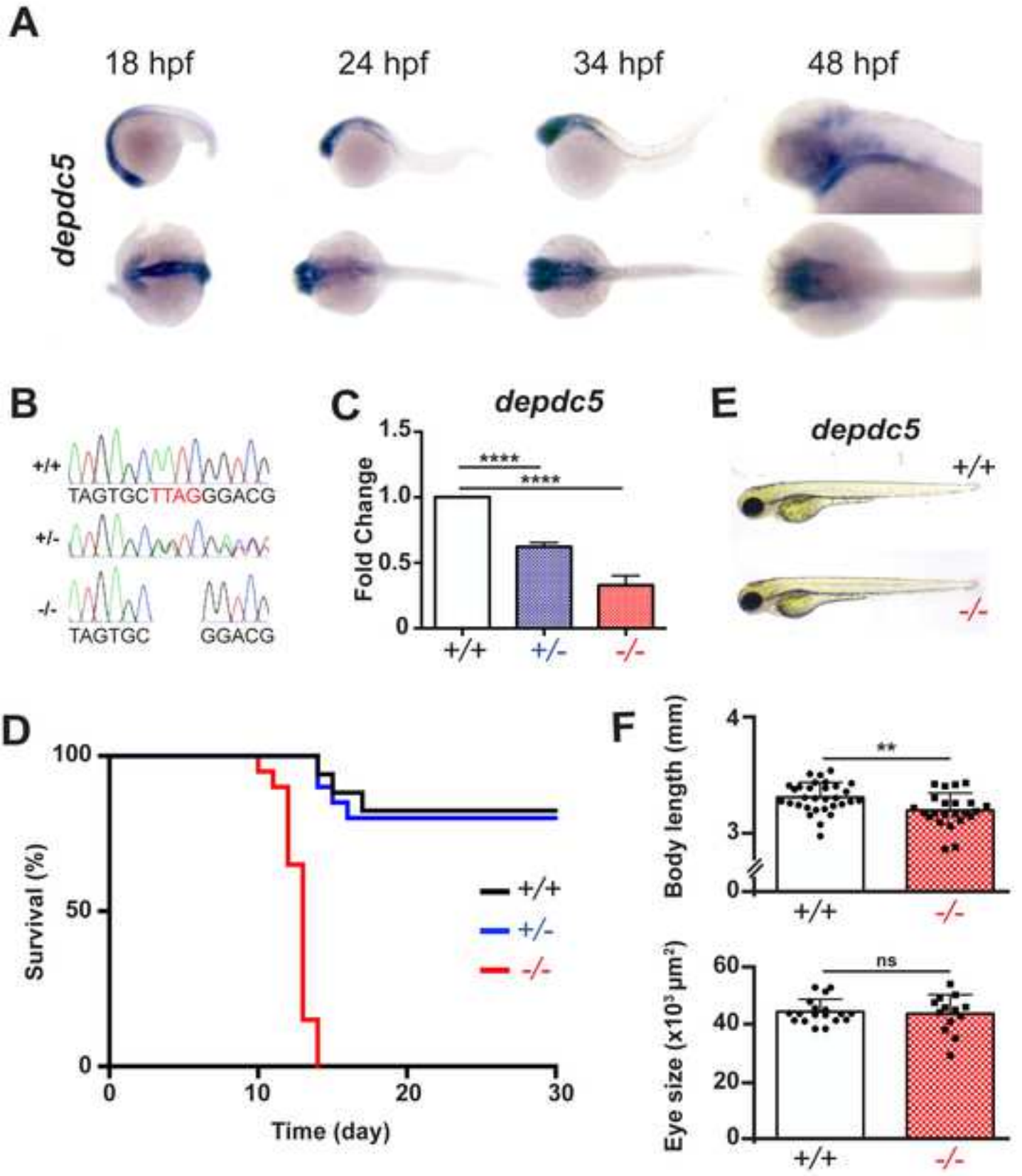

Figure 2

Click here to download Figure Fig 2.tif

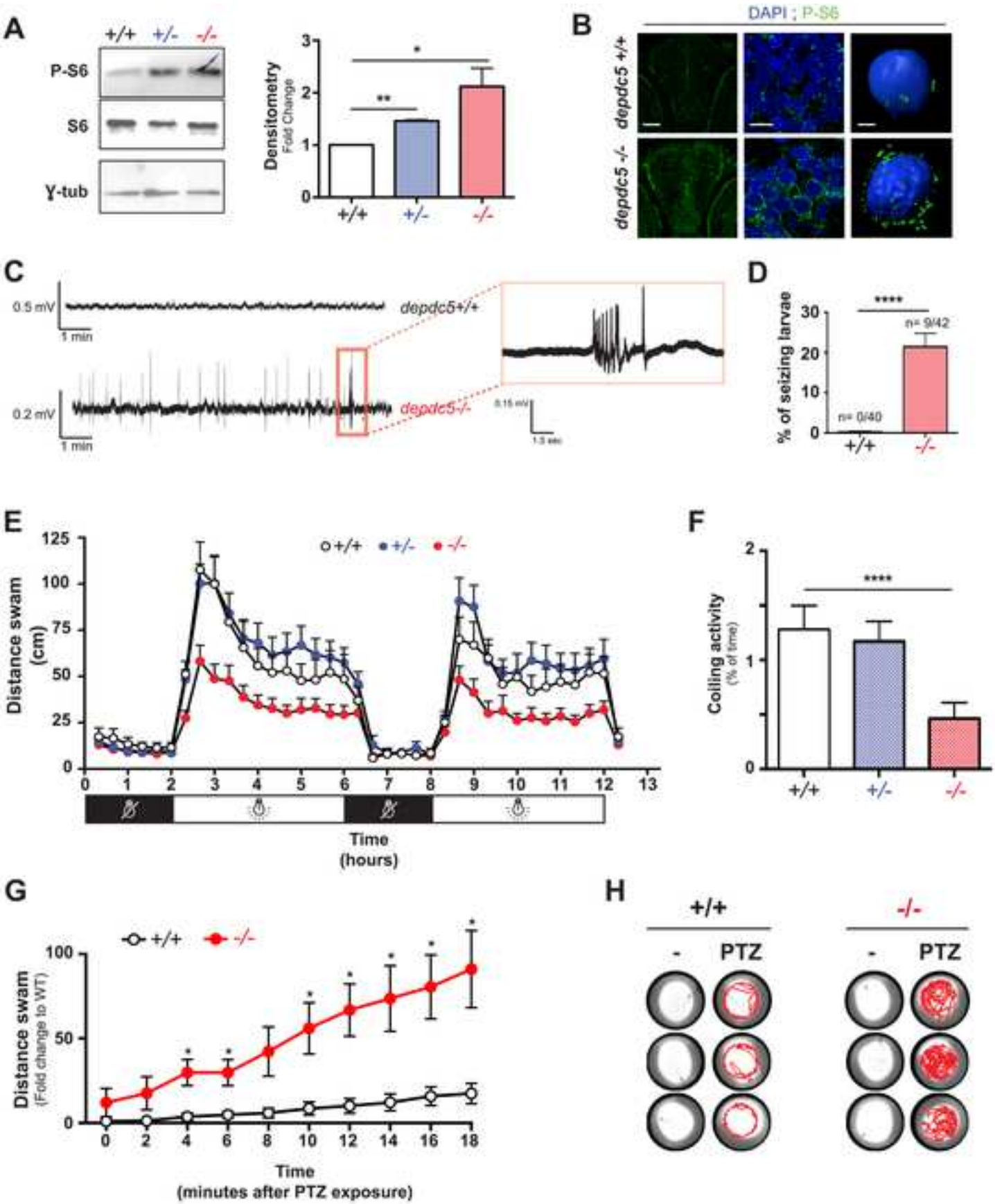

Figure 3

Click here to download Figure Fig 3.tif

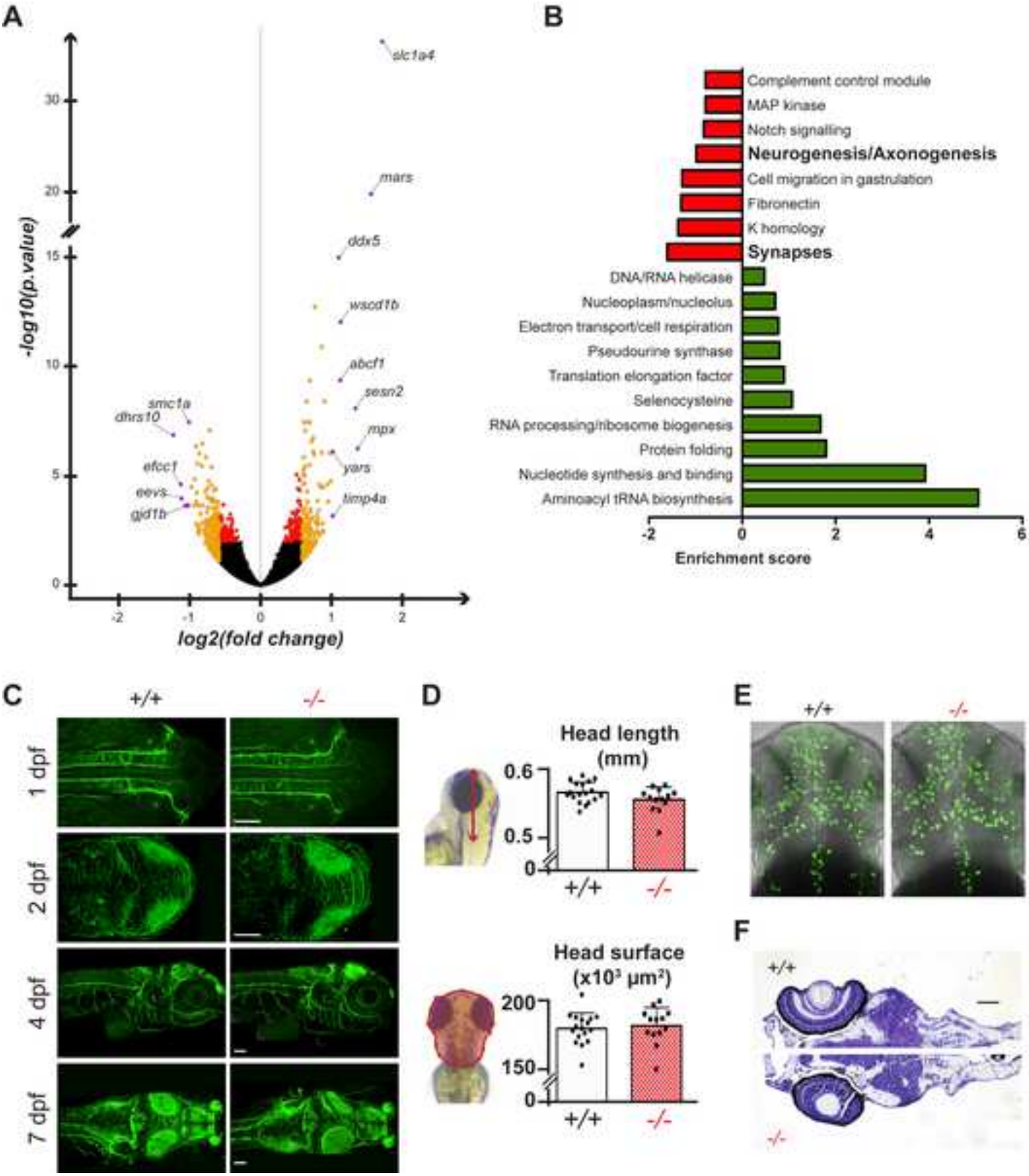

Figure 4

Click here to download Figure Fig 4.tif

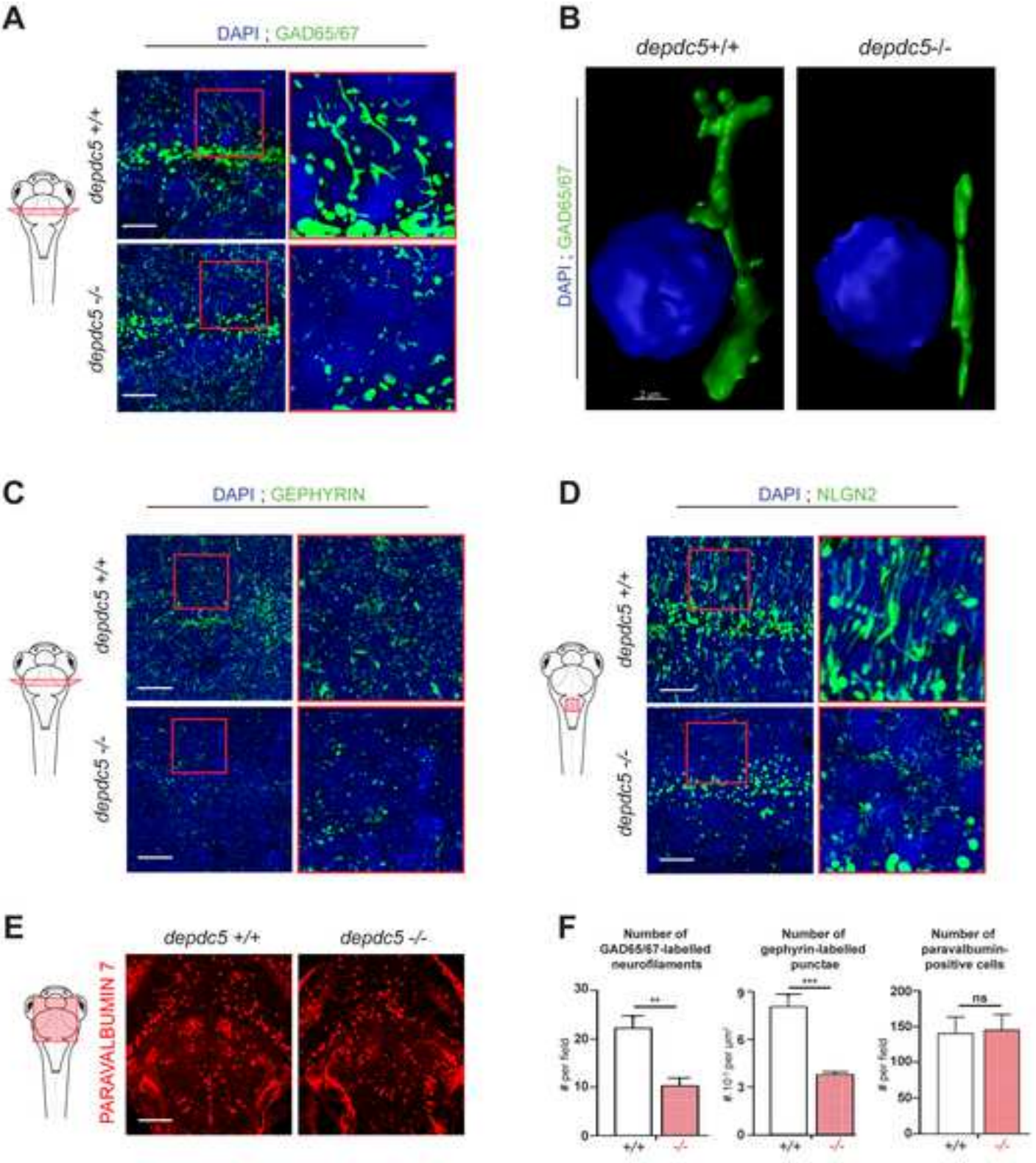

Figure 5

Click here to download Figure Fig 5.tif

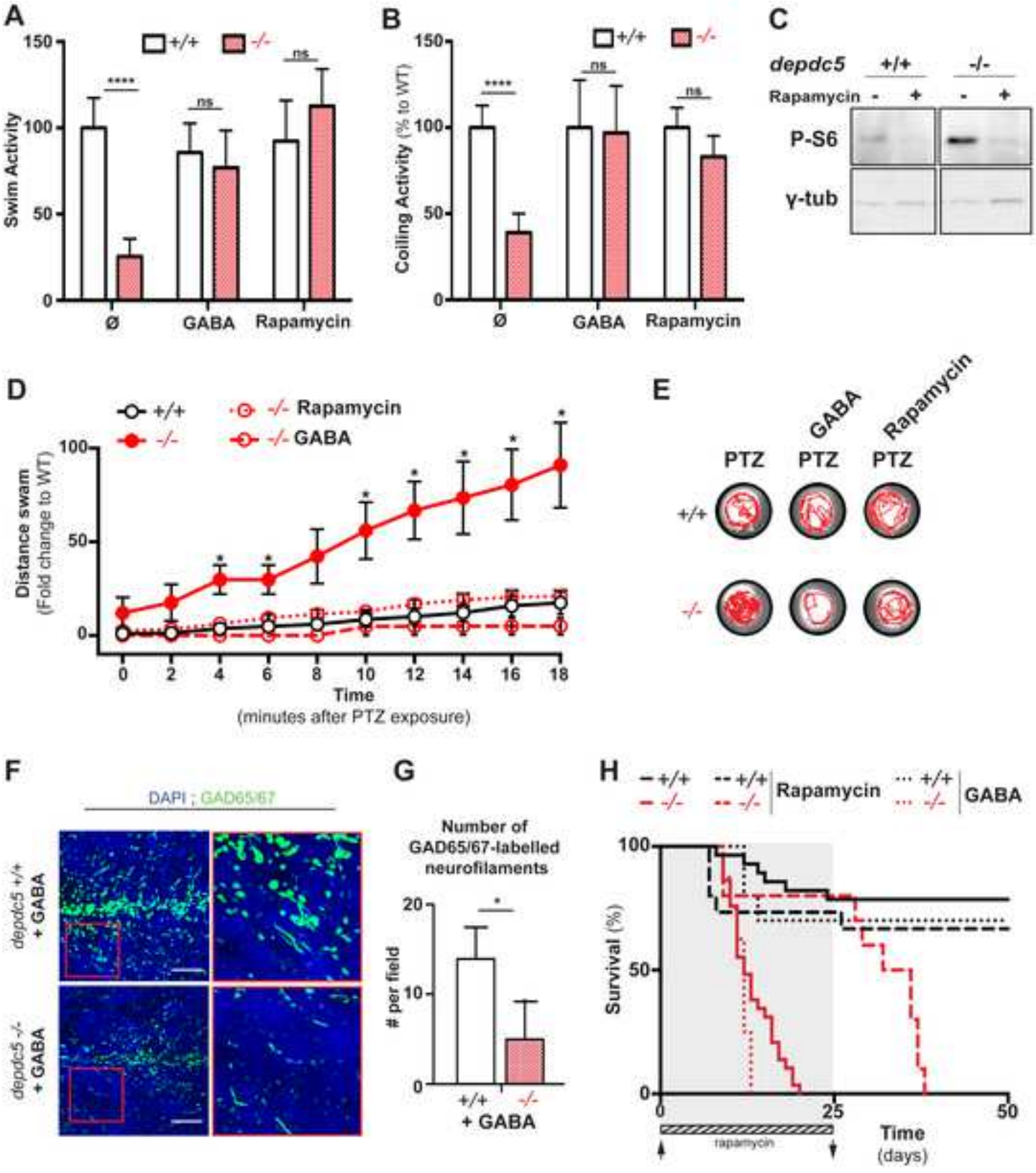

Figure 6

Click here to download Figure Fig 6.tif

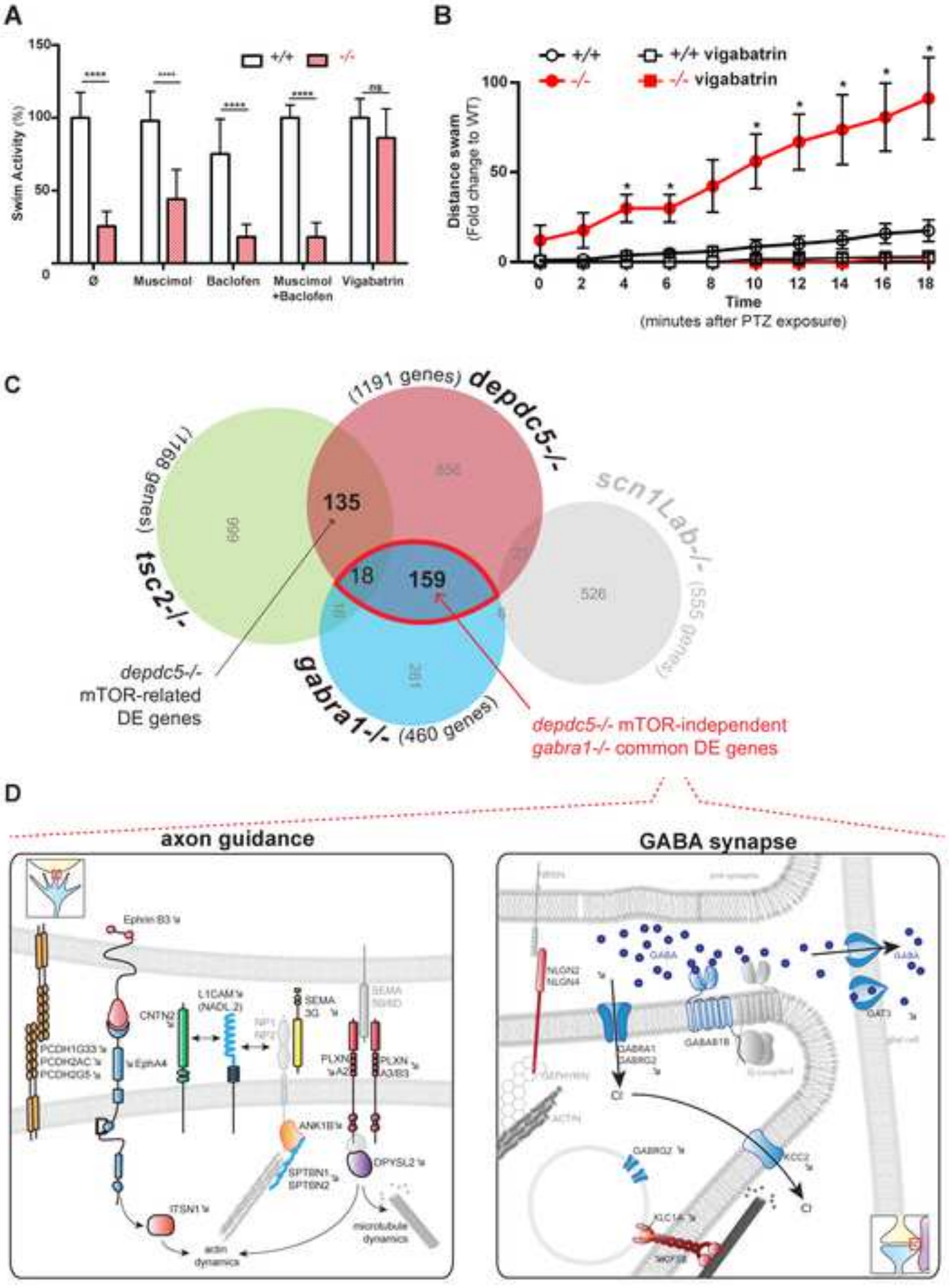

Figure 7

Click here to download Figure Fig 7.tif

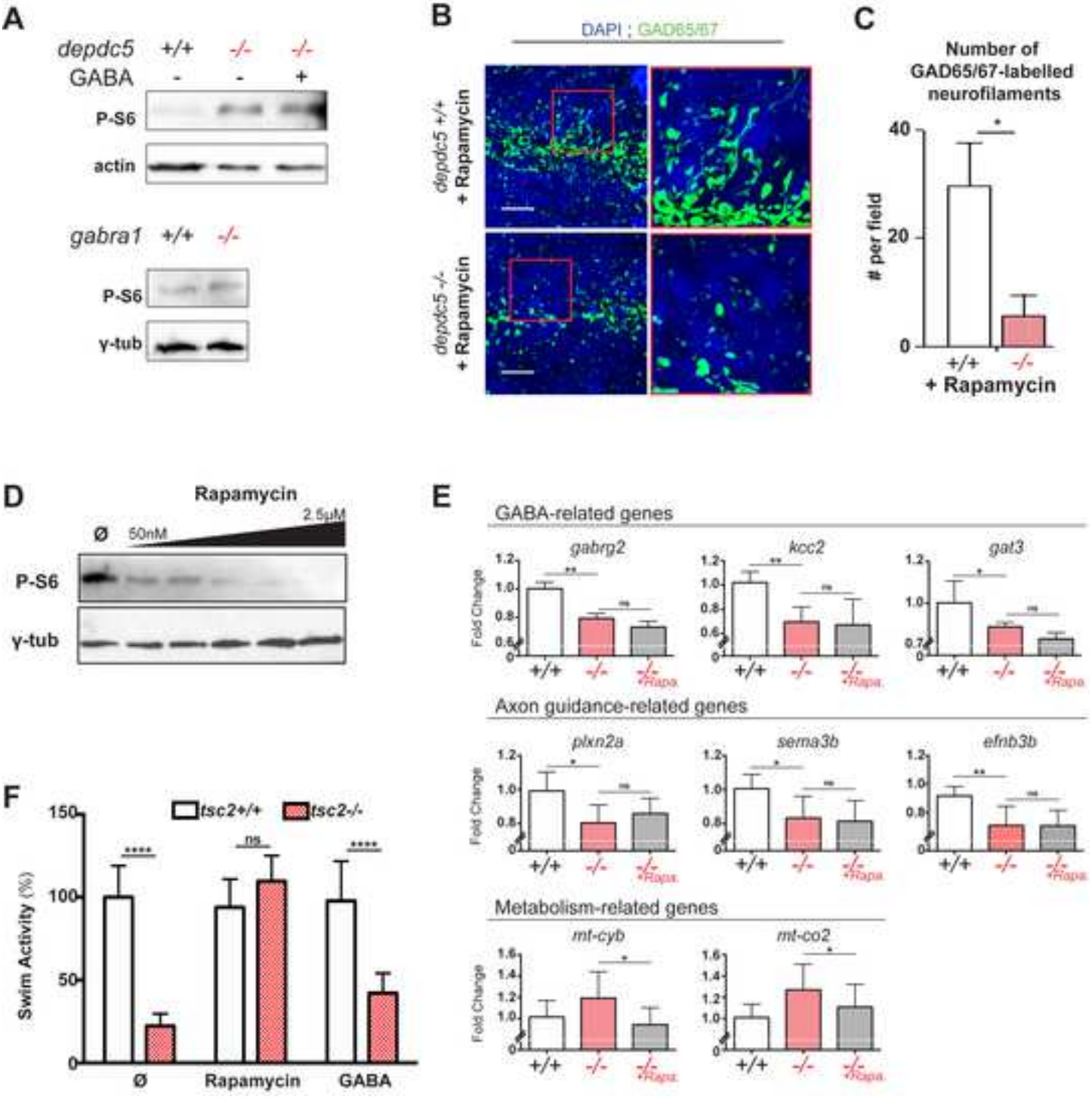

Table S1

Click here to access/download

Supplemental Videos and Spreadsheets

Table S1.xlsx

Table S2

Click here to access/download

Supplemental Videos and Spreadsheets

Table S2.xlsx

Table S3

Click here to access/download

Supplemental Videos and Spreadsheets

Table S3.xlsx

Table S4

Click here to access/download

Supplemental Videos and Spreadsheets

Table S4.xlsx

Supplemental Video

Click here to access/download

Supplemental Videos and Spreadsheets

video S1.mp4

Supplemental Video

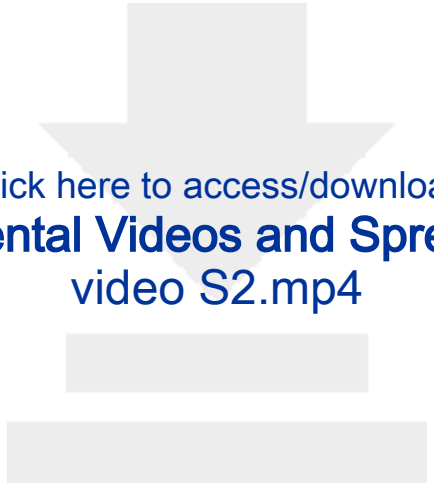

Click here to access/download

Supplemental Videos and Spreadsheets

video S2.mp4